

# Origin of the Badar Sand Field and the late pleistocene tectonic movements in the Tunka depression, the Baikal Rift Zone, Eastern Siberia

A.A. Chebotarev<sup>a,\*</sup>, S.G. Arzhannikov<sup>a</sup>, A.V. Arzhannikova<sup>a,b</sup>, R.N. Kurbanov<sup>c,d</sup>

<sup>a</sup> Institute of the Earth's Crust, Russian Academy of Sciences, Siberian Branch, 664033, Lermontova str., 128, Irkutsk, Russia

<sup>b</sup> Geological Institute, Russian Academy of Sciences, Pyzhevsky lane, 7, bld. 1, Moscow 119017, Russia

<sup>c</sup> Lomonosov Moscow State University, Faculty of Geography, 119991, Leninskiye Gory, 1, Moscow, Russia

<sup>d</sup> Institute of Geography, Russian Academy of Sciences, 119017, Staromonetniy lane, 29, Moscow, Russia

## ARTICLE INFO

### Keywords:

Baikal Rift Zone  
Tunka Basins  
Pleistocene sedimentation  
Badar Sand Field  
Delta sand sediments  
OSL dating  
Dammed lake

## ABSTRACT

The Badar Sand Field is a geomorphological phenomenon representing a dome structure that dominates the topography of the subsiding Tunka Depression in the SW Baikal Rift. Many interpretations of its origin, including tectonic uplift, have been proposed, but the question remains open. We propose a new model to explain its genesis, based on a thorough analysis of both new and previously published geomorphological and sedimentological data. We suggest that the accumulation of the Badar Sand Field occurred in two stages: aquatic and aeolian. The lower part of the sandy deposits accumulated during the long-term existence of a landslide-dammed paleolake within the Tunka Depression. The upper part was formed after the drainage of the paleolake due to aeolian redeposition of sands. New results of OSL-dating from the vertical 40-m geological cross-section "Badar" showed that the accumulation of lake sediments occurred in the period 24–15 thousand years ago (MIS2). Based on the analysis of satellite images, we modeled the paleolake and determined that it arose as a result of landslides that dammed the antecedent section of the Irkut river valley in the Elovsky Spur. The analysis of the Irkut river terraces showed the absence of tectonic uplift within the Tunka Depression in the Holocene. The incision of the Irkut River at 40–90 m into the Badar dome occurred as a result of the restoration of equilibrium in the longitudinal profile of the river due to changes in sedimentation conditions in the post-glacial period.

## 1. Introduction

The Tunka Basins (TBs) (Fig. 1 B, C) are part of the intracontinental Baikal Rift Zone. These basins on the southwestern side of this rift zone are structurally located in a transitional zone between a compressional deformation zone of the Western Mongolia and a tensile deformation zone of the central part of the Baikal Rift Zone. The Tunka Basins consist of a series of small depressions: Mondy, Khoytolog, Turan, Tunka, Tory and Bystraya. These depressions developed in the mode of transtensional deformations starting from the Oligocene, which intensified in the late Pliocene due to the propagation of compressive deformations to the north, as a result of the India-Asia collision (e.g. Larroque et al., 2001; Arzhannikova et al., 2011; Jolivet et al., 2013). The normal Tunka Fault controls the subsidence of the TBs. Morphotectonic studies and the study of the evolution of stress fields showed a change in the deformation regime in the late Pleistocene from transtensive to transpressive

(Parfeevets and San'kov, 2006; Larroque et al., 2001). This led to the uplift of some parts of the TBs and to the reverse-slip kinematics of the Mondy, the eastern segments of the Tunka and Main Sayan faults (Chipizubov et al., 2003; Shchetnikov and Ufimtsev, 2004; Arzhannikova et al., 2004; Ufimtsev et al., 2009; Ritz et al., 2018; Arzhannikova et al., 2018; Arzhannikova et al., 2023) (Fig. 1 C). In the distal parts of the TBs (Mondy and Bystraya depressions), the Neogene deposits are strongly incised which indicates the tectonic uplift of the basins. At the same time, the central part of the TBs continued subsidence during the Quaternary period. According to drilling data (Highlands of the Baikal region, 1974), Neogene deposits of the TBs are overlain by Quaternary deposits 400–500 m thick. Quaternary deposits consist of alluvial, proluvial and lacustrine-swamp sediments. There are a number of problems in the interpretation of geological and geomorphological data concerning the Late Quaternary sediments of the Tunka Depression. On the one hand, the meandering of the rivers and swampy areas in the basin (e.

\* Corresponding author.

E-mail addresses: [che@crust.irk.ru](mailto:che@crust.irk.ru) (A.A. Chebotarev), [arzhan@crust.irk.ru](mailto:arzhan@crust.irk.ru) (S.G. Arzhannikov), [sarzhan@crust.irk.ru](mailto:sarzhan@crust.irk.ru) (A.V. Arzhannikova), [kurbanov@igras.ru](mailto:kurbanov@igras.ru) (R.N. Kurbanov).

<https://doi.org/10.1016/j.jseaes.2023.105957>

Received 19 July 2023; Received in revised form 15 November 2023; Accepted 28 November 2023

Available online 1 December 2023

1367-9120/© 2023 Elsevier Ltd. All rights reserved.

g. Koimorskaya lowland) indicate the continued subsidence of the basin. On the other hand, some landforms, such as high sand fields (e.g. Badar Sand Field (BSF)), do not fit into the model of the subsiding depression of the basin, and are interpreted by some researchers as evidence of its inversion rise (Ufimtsev et al., 2009; Shchetnikov, 2017).

Badar Sand Field is located in the central part of the Tunka Depression (Fig. 1 C). The surface of the BSF is 40–130 m higher than the modern floodplain of the Irkut River and its tributaries, which drain the Tunka Depression.

Thus, the obtained data of previous studies did not create a general coherent concept of the BSF formation in the inner part of the Tunka Depression. The age estimations of the sand sediments for different fields do not correlate with each other. Various researchers propose different depositional environments based on the results of palynological, sedimentological, paleoclimatic analyzes (Martinson, 1948; Logachev, 1958; Bulmasov, 1963, 1967; Zamaraev, 1975; Osadchy, 1995; Kolomiets, 1998, 2019; Matz et al., 2002; Ufimtsev et al., 2003; Vogt and Vogt, 2007; Isaev, 2007, 2016; Krivonogov, 2010, Krivonogov and Safonova, 2017; Semeny et al., 2014, 2015; Shchetnikov, 2017 Maksimov et al., 2020). Today, several different versions of the genesis and age of the Badar Sand Field are known.

According to existed data (Logachev, 1958), the origin of the sands is not related to the Baikal transgression. The time of the sands formation associate with prolonged strong glaciation. The sands in the central part of the depression are represented by facies of shallow lakes. In the marginal parts of basin there are alluvial facies with a combination of obliquely and parallel layers. The conditions of sand formation in the system of cold migrating lakes are characteristic of glacial epochs, when lakes were fed by seasonal melting of glaciers.

Bulmasov (1963, 1967) assumed the cryogenic version of the sand dome formation. In that case, BSF is a cryogenic structure, i.e. an ice core that has surfaced among melted sediments due to the low specific density of permafrost. This is the process of establishing an isostatic

equilibrium between the frozen deposits of lower density and the subsiding deposits of the basin.

Zamaraev (1975) proposed to consider the BSF as a gravitational fold, which was formed as the sliding of the Tunka Depression deposits on the inclined surface of the foundation on the northern wing of the Tunka Fault (by analogy with the gravitational structures on the underwater slope of the Southern Baikal Basin). Gravity-driven slumping is a characteristic of heavily watered sediments experiencing isostatic deformations during tectonic events, being realized in the form of gravitational collapse structures.

According to another viewpoint (Osadchy, 1995; Kolomiets, 1998; 2010; 2019 etc.) the formation of sandy sediments in Baikal Rift basins is the result of the ingress of Baikal waters into it due to a rise of Lake Baikal water level (Matz et al., 2002). A low-flow reservoir was formed in the Tunka Depression, which led to the accumulation of sand deposits. A comprehensive analysis of the composition of sediments using established relationships and patterns between various hydrodynamic indicators allowed researchers to reconstruct the parameters of the river flow that transported and deposited sandy material (Kolomiets, 2019).

The accumulation of BSF could be carried out in a calm environment of lake-alluvial conditions, as well as turbulent river and bottom currents with seasonal fluctuations in water content. Such conditions correspond to the situation in the coastal strip of the water area of lake flowing reservoirs. Evidence of the existence of such reservoirs in the Tunka Depression is the remnants of sponges and malacofauna (Martinson, 1948; Logachev, 1958).

Kolomiets (2019) proceeded from the data of the age of the sand at least 65 ka (Ufimtsev et al., 2003). However, the time of the last significant rise of Lake Baikal level cannot be younger than 130 ka (Arzhannikov et al., 2018; Arzhannikov et al., 2021a,b). An additional limitation for TSB is the tectonic uplift of the marginal eastern part, which has been rising since the late Pleistocene, and since that time has significantly exceeded the Angara outlet. There are also versions of the

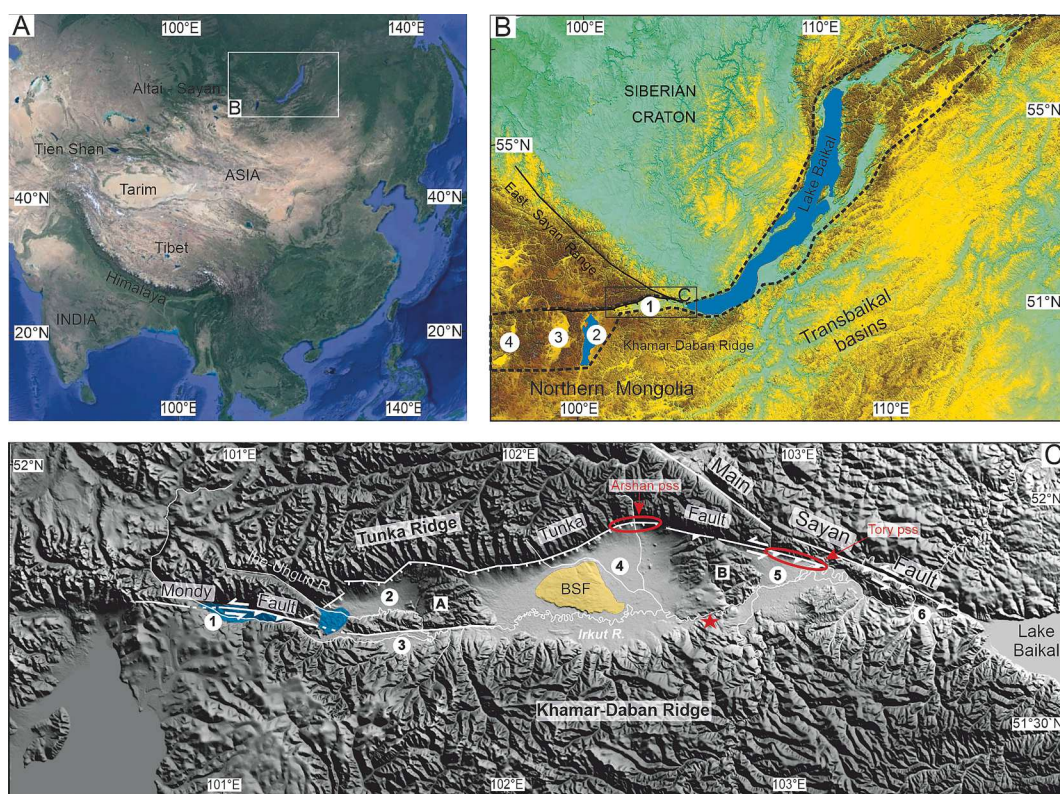


**Fig. 1.** A series of maps showing the location of the study area. A - Simplified map of Asia; B - the map showing main relief elements of the Baikal Rift Zone; C - elevation of the Tunka Basins (TBs) and the main elements of the morphostructure mentioned in this article.

aeolian origin of the BSF (Krivonogov, 2010), a domed anticline uplift (Ufimtsev et al., 2009), a version of a mud volcano (Isaev, 2007, 2016). These versions are rather poorly reasoned and not supported by research data.

Thus, for the entire period of the BSF study, a large amount of disparate data was obtained. However, there is still no consensus in the scientific community about the genesis and age of the sand sediments. The age of the BSF deposits is represented by only one date and is controversial. Signs of the basement inversion in the marginal parts of the TBS in the late Pleistocene are obvious, but the question remains whether the uplift occurred in the central part of the Tunka Depression. In this paper, we present the results of a detailed sedimentological study and OSL-dating of the BSF, which allowed us to clarify the genesis and age of this geomorphological phenomenon. We also analyzed terrace heights, studied and dated alluvial deposits of the Irkut River in several sections along the Tunka Depression to understand the post-Badar depositional environment. In combination with data from previous studies performed on other sections of high sandy deposits of the TBs, our results allowed us to present a new model of Late Quaternary sedimentation in the Tunka Depression and consider the possibility of its uplift compared to other causes of deep incision into the sediments of the basin.

## 2. Overview of ideas about the genesis of the Baikal Rift Zone's sand fields

Our research focuses on the study of sand deposits. Therefore, we present some characteristics of the sand fields of the Baikal Rift Zone for a more complete understanding of their genetic diversity.

Sand fields are widespread within the BRZ. They can make up to 2/3 (Logachev, 1968) of the volume of Quaternary sediments and are represented in the Hovsgol, Tunka, Barguzin, Muya, Upper Angara and other basins (Fig. 2).

The sands occupy the central and peripheral parts of the basins, sometimes spreading high on the slopes of the mountain ridges. The question of the sand deposit formation in the BRZ was studied by different researchers (Logachev, 1958; Bulmasov, 1963; Ravsky et al., 1964; Zamaraev, 1975; Adamenko et al., 1975; Kul'chitsky et al., 1994; Osadchy, 1995; Kolomiets, 1994, 2010; Ufimtsev et al., 1999, 2003; Vogt and Vogt, 2007; Krivonogov, 2010; Krivonogov and Safonova, 2017; Semeny et al., 2014, 2015; Maksimov et al., 2020). They found that the origin of the sands in the depressions of the BRZ is associated

with different processes dictated by local structural and climatic conditions.

For example, the sand fields of the Tchara Basin (northeast extremity of the BRZ (Fig. 2)) were formed in the front of glaciers or as an avandelta in a proglacial dammed lake, at different times of the late Pleistocene (Enikeyev, 2019).

Sandy deposits (up to 400–500 m according to drilling data) in the Barguzin and Upper Angara basins have a fluvio-glacial structure due to the large terminal moraines of the Barguzin and Upper Angara ridges (Logachev, 1958).

In the Muya Basin, a large sedimentary sand field was accumulated in the Vitim glacial dammed lake (Margold et al., 2018).

In some basins of Transbaikalia, in the structure of floodplain terraces, there are deposits of lacustrine strata associated with the transgression of Lake Baikal (Kolomiets, 2021). The genesis of sands in the TBs is different. For example, there is a 150 m high sand dune located on the surface of a 12 m terrace in the Khoytogol depression (Fig. 3). Its genesis is defined as aeolian (Ufimtsev et al., 2003). In the Bystraya Depression, the sands are represented by both terrace sediments of the Irkut River and fragments of ancient alluvial deposits, raised to the surface as a result of late Pleistocene uplift (Hassan et al., 2021) (Fig. 3). In the Tory Depression, dunes cover the northern gentle slope of the Hamar-Daban Ridge as a result of the aeolian transporting (Ravsky et al., 1964) (Fig. 3). On the other hand, there are horizontally layered sands of lacustrine genesis overlapping river alluvium in the terraces of the inner part of the Tory Depression (Ravsky et al., 1964). In the Turan Depression, the sands have lacustrine-alluvial genesis, but the upper part is overlain by subaerial Holocene sand (Ravsky et al., 1964, Osadchy, 1995).

## 3. Geological setting

### 3.1. Brief tectonic history

The Tunka basins are located between the mountainous of Northern Mongolia in the south and the East Sayan Ridge in the north (Fig. 1B). It forms the southwestern flank of the Baikal Rift together with the Hovsgol, Darhat and Busingol basins (Fig. 1B). The Tunka basins are represented by a system of half-grabens, extending from east to west for 170 km. This segment of the Baikal Rift includes a chain of local depressions (from west to east: Mondy, Khoytogol, Turan, Tunka, Tory, Bystraya) filled with Oligocene-Quaternary sediments (Logatchev and

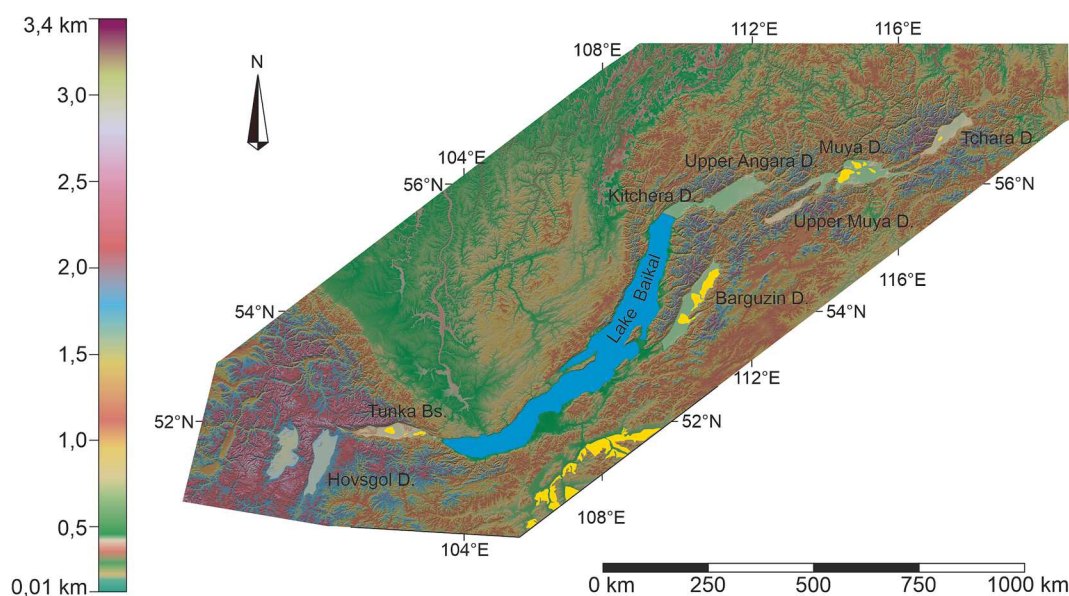
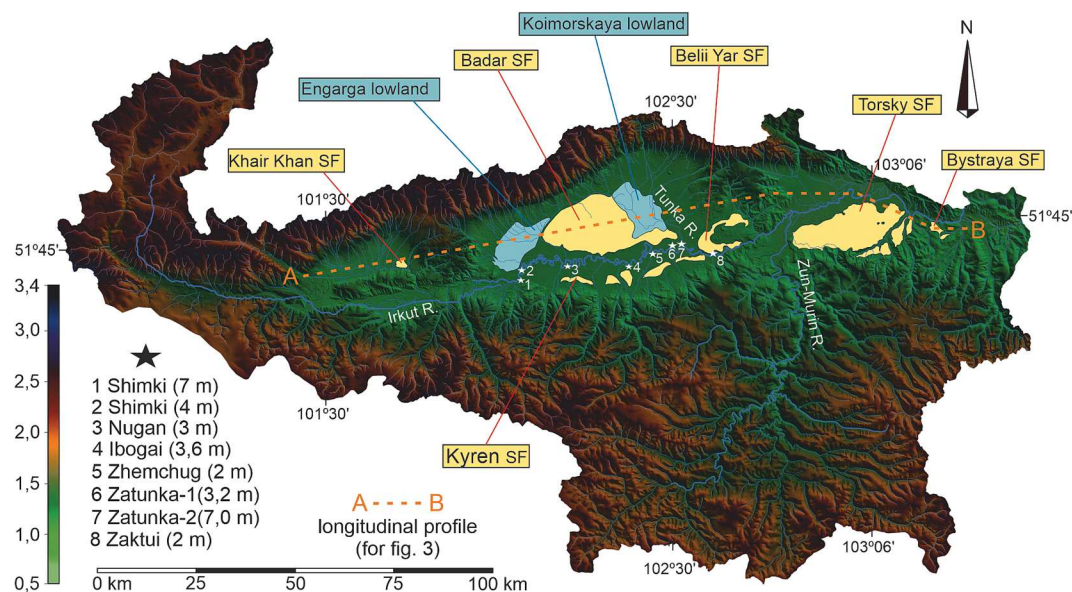


Fig. 2. The Baikal Rift Zone and location of Late Quaternary sand fields.



**Fig. 3.** The map shows the location of the Tunka Basin system (TBs) within the catchment boundaries of the Irkut River drainage system and its tributaries. Sand Fields (SF) are marked in yellow and lowland are marked in blue. The stars show the sections of the Irkut River terraces. (For interpretation of the references to color in this figure legend, the reader is referred to the web version of this article.)

Zorin, 1987). Interbasin spurs (Kharadaban, Nilovsky and Elovsky) separate the depressions (Fig. 1 C). The Tunka Ridge (3000–3200 m asl) bounds TBs from the north and Khamar-Daban Ridge (2200–2400 m asl) from the south.

The subsidence of the TBs began in the Oligocene, when fine-grained lacustrine - swamp sediments accumulated (Mazilov et al., 1972). The Tunka Fault became active at the end of the Miocene, which led to an increase in the rate of subsidence of the basin and the beginning of the accumulation of coarse-grained sediments. Since that time, the Tunka Depression has acquired outlines close to modern ones (Mazilov et al., 1972). The age of activation of the Tunka fault is about 3.5 million years according to the morphometric analysis of the fault ledge (Chebotarev et al., 2021). Subsidence of TBs and the activation of the Tunka Fault coincide with the period of active mountain formation in the Baikal-Mongolian region associated with the northward propagation of compression deformations from the India-Asia collision (Molnar & Tapponnier, 1975; Zonenshain & Savostin, 1981; Jolivet et al., 2009, 2013; Arzhannikova et al., 2011). The development of the TBs at this time occurred in the transension mode, in which the Tunka Fault was deformed as a normal left-lateral strike-slip (Larroque et al., 2001).

The pattern of tectonic stress fields for the Tunka segment of BRZ changed in the late Pleistocene. Since that time, movements along some fault segments have been demonstrating a change in the regional deformation regime from transension to transpression (Ritz et al., 2018; Parfeevets and San'kov, 2006; Larroque et al., 2001). The inversion affected the sublatitudinal segments of the Tunka, Sayan and Mondy faults located at the western and eastern ends of the TBs (Fig. 1 C). This became known after studying paleo-earthquake deformations in this area (Arzhannikova, 2004, 2022; Ritz et al., 2018; Chipizubov and Smekalin, 1999, 2003). The traces of paleoearthquakes studied on the Tunka Fault in the Tory Depression (east of TBs) and on the Elovsky Spur are also interpreted as a left-lateral displacements associated with a reverse component (Chipizubov et al., 2003) (Fig. 1 C). Concurrently, the Arshan seismic site in the Tunka Depression is classified as a left lateral normal fault (Chipizubov et al., 2003; Smekalin, 2008; Arzhannikova et al., 2018) (Fig. 1C). Thus, young low-amplitude inversion uplifts associated with paleoseismic events of magnitude  $\geq 7.5$  are recorded inside the TBs against the background of general subsidence characteristic of rift depressions. Inversion is a consequence of compression processes and is accompanied by erosive cutting of Quaternary

sediments and exhumation of Neogene sedimentary formation of the marginal basins. Some authors (Ufimtsev et al., 2002; Shchetnikov, 2017) believe that the central Tunka Depression, together with the marginal ones, was also involved in the tectonic inversion.

### 3.2. Sedimentation of the Tunka basin system

Tunka basins have different amplitudes of subsidence according to geophysical data and drilling of sedimentary deposits (Sherman et al., 1973; Mazilov et al., 1972) (Fig. 4). A significant difference in the thickness of the sedimentary filling indicates the distinctive conditions and duration of the formation of the basins (Mats, 1993; Logachev, 2003). Thus, the thickness of sediments in the Khoitogol and Tory depressions does not exceed 500–600 m. In the Tunka Depression the thickness is 2800 m (Sherman et al., 1973) (Fig. 4).

The Tunka Depression sediments are the most studied due to intensive well drilling in the 2nd half of the 20th century associated with the search for coal in Neogene deposits and scientific research (Sherman et al., 1973; Hassan et al., 2020). We present a summary description of the sediment based on drilling data and the study of open sections of the Tunka Depression (Sherman et al., 1973; Rasskazov et al. 2010; Shchetnikov et al. 2012) (Fig. 5). Two stratigraphic complexes associated with different stages of Baikal rifting (Logachev, 1968; Logatchev and Zorin, 1987) represent the sediments of the basin. The lower part (the stage of “slow rifting”) was accumulated during the subsidence of the basin in the Oligocene-Miocene. It consists of lacustrine-swamp and river facies: sandstones, siltstones and clays interspersed with several generations of basalt lava.

The upper part is composed of coarser deposits of the “fast rifting” stage (Logachev, 1968; Logatchev and Zorin, 1987) with a wide genetic spectrum (lake, river, proluvial, slopewash, avalanche, landslide, glacial, fluvioglacial, aeolian, etc.) (Logachev, 1968; Ravsky et al., 1964). (Fig. 5). This part was accumulated in the Late Pliocene–Pleistocene, during the intensification of tectonic movements and it is divided into two strata: ochre molasse and overlying gray molasse. Gray molasse contains thick deposits of polymictic sands. It occupies up to 2/3 of the volume and a significant area of Pleistocene-Holocene deposits in all depressions of the TBs. The sands upper level is located at an altitude of 40–100 m or more above the modern bed of the Irkut River (Ufimtsev et al., 2002). Sands are replaced by gravel, pebble or coarse-grained

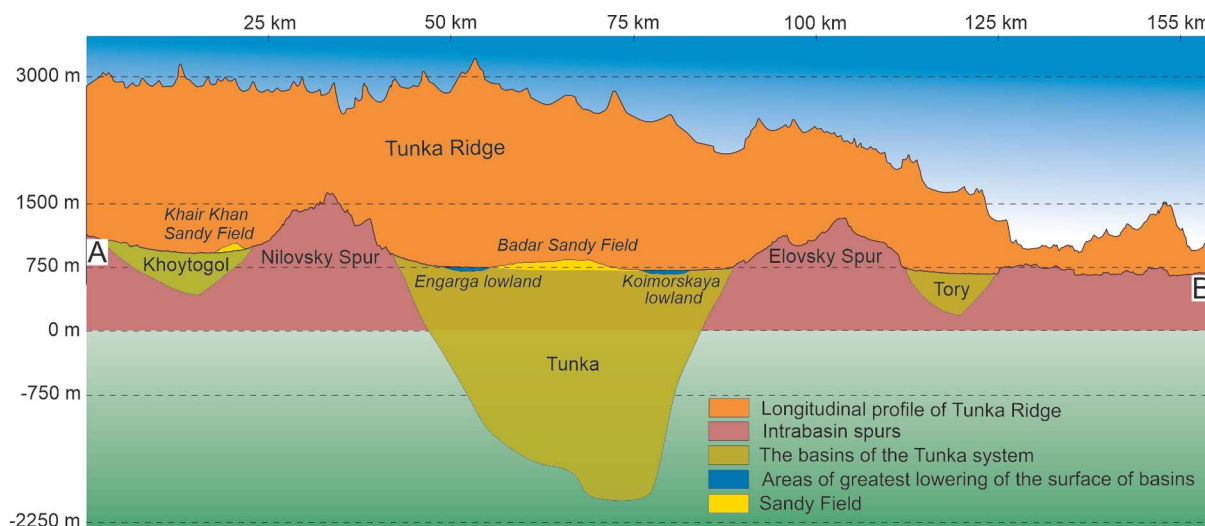


Fig. 4. The longitudinal profile of the Tunka Depression with the main structural elements (location of profile A-B in Fig. 2).

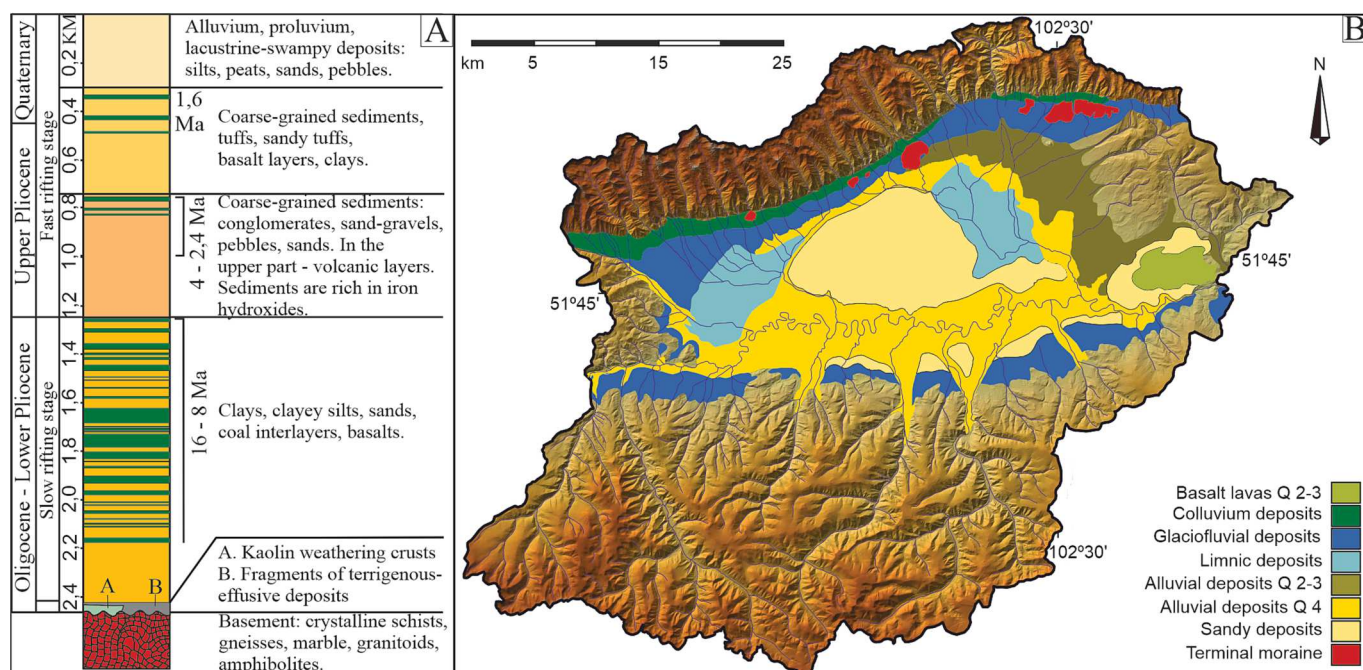


Fig. 5. A - Stratigraphic column of the Tunka Depression sediments (modified after Shchetnikov et al. (2012) and Rasskazov et al. (2010)); B - the map showing simplified quaternary volcanic rocks and sediments of the Tunka Depression (VSEGEI, 1965, 1966, 1969).

slope deposits on the periphery of the basins. These sediments form a piedmont along the Tunka Ridge together with colluvium and terminal moraines. According to the surface exposure dating (10Be) of the boulders of terminal moraines in the south of the Eastern Sayan, the average age of the youngest terminal moraines is 16–14 thousand years ago. (Arzhannikov et al., 2012, 2015).

### 3.3. Late Quaternary sand fields of the Tunka Depression

The main elements of the Tunka Depression relief are the erosive-accumulative valley of the Irkut River with a width of 5–6 km; an accumulative plain partially overlain by aeolian dunes; an accumulative piedmont of the Tunka Ridge; and Badary Sand Field (Fig. 5 B). The Irkut Valley has a relatively flat surface with a wide belt of meanders, with elevation differences along the bottom from 760 m asl in the west to 705 m asl in the east. The slope areas of Tunka Depression are formed by

glacial, fluvioglacial, proluvial deposits. Three large sandy fields with varying degrees of exploration are known in the Tunka Depression: Belyi Yar, Kyren and Badary. They are located in different parts of Tunka Depression, but in geomorphological terms, they look like parts of one large sandy field eroded by the Irkut and Tunka rivers and partially transformed by aeolian processes (Fig. 3).

#### 3.3.1. Belyi Yar

Belyi Yar is a large sandy field with a thickness from 15 to 26 m, exposed by lateral erosion of the Irkut River. The sediments were studied in two sections – Belyi Yar – 1 (BY-1) and Belyi Yar – 2 (BY-2), located at a distance of 2 km from each other (Ravsky et al., 1964, Ravsky, 1972; Adamenko et al., 1975, 1984; Popova et al., 1989; Kul'chitsky et al., 1994; Maksimov et al., 2015; Shchetnikov et al., 2015) (Fig. 6). The deposits are represented by two facies. In the lower part of the section, there are lacustrine-swamp sediments (interlayer of peat, weakly

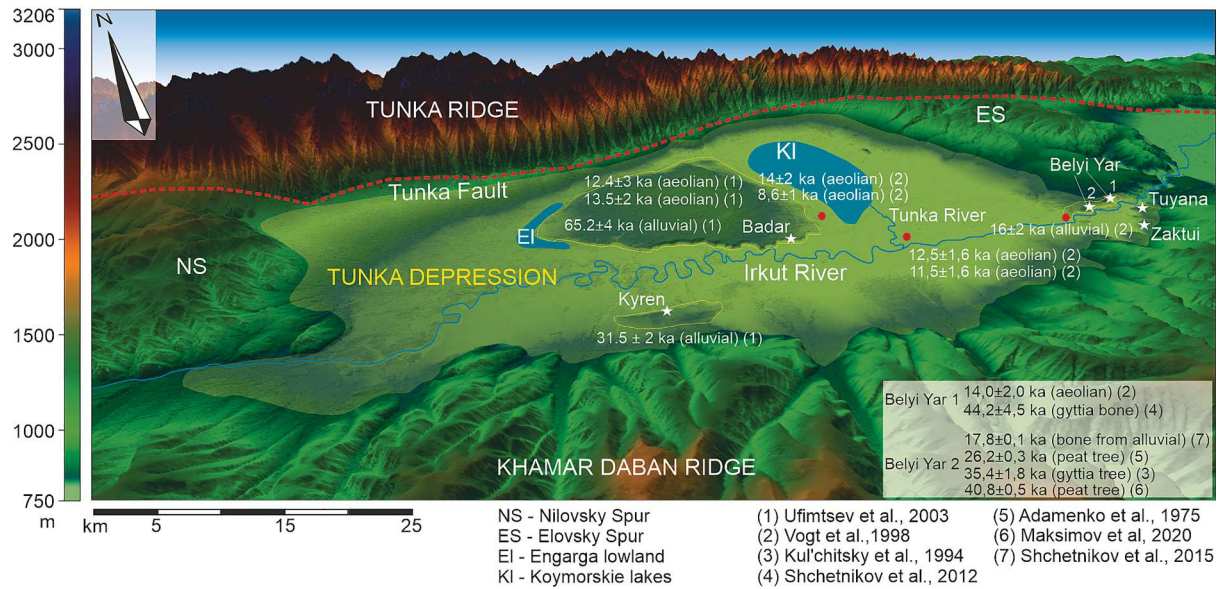


Fig. 6. The map highlights the currently known AMS and TL dates of sand deposits in various geomorphological objects (white stars) of the Tunka Depression.

ferruginous siltstones and sandy gyttia) with organic material (Fig. 7). This part of the sediments is well characterized by palynological, paleocarpological studies and analysis of malacofauna (Ravsky et al., 1964, Ravsky, 1972; Adamenko et al., 1975, 1984; Popova et al., 1989; Kul'chitsky et al., 1994). Three <sup>14</sup>C dates were obtained from peat paleosol: 30040–31038 cal year BP (Adamenko, 1975), 40680–44396 and 41234–42954 cal year BP (Maksimov et al., 2015), which correspond to the MIS 3. Horizontal and cross-bedded sands overlie these sediments. The sands are interbedded in the lower part with poorly rounded gravel and small pebbles (Ravsky et al., 1964). The genesis of sands at different depths of the section is interpreted as channel alluvium, floodplain,

lacustrine, swamp facies (Ravsky et al., 1964; Semenyev et al., 2014). A large number of mollusk shells from the sandy deposits of BY-2 are interpreted as terrestrial and freshwater (Ravsky et al., 1964). The age of sand deposits in the upper part of the section (from 16 to 2 m depth on the BY-1 and from 12 to 2 m on the BY-2) corresponds to the MIS 2 (Adamenko et al., 1975; Kul'chitsky et al., 1994; Shchetnikov et al., 2015). Non-stratified sands and loess-like sandy loams of aeolian origin overlie the sandy strata of the aquatic genesis. Its age was determined by thermo-luminescent (TL) method as 16120 ± 3580 and IRSL method as 16120 ± 2730 (a sample from a depth of 2 m). At a depth of 1.7 m, the age of the aeolian deposits according to TL 14110 ± 2670, IRSL 14030

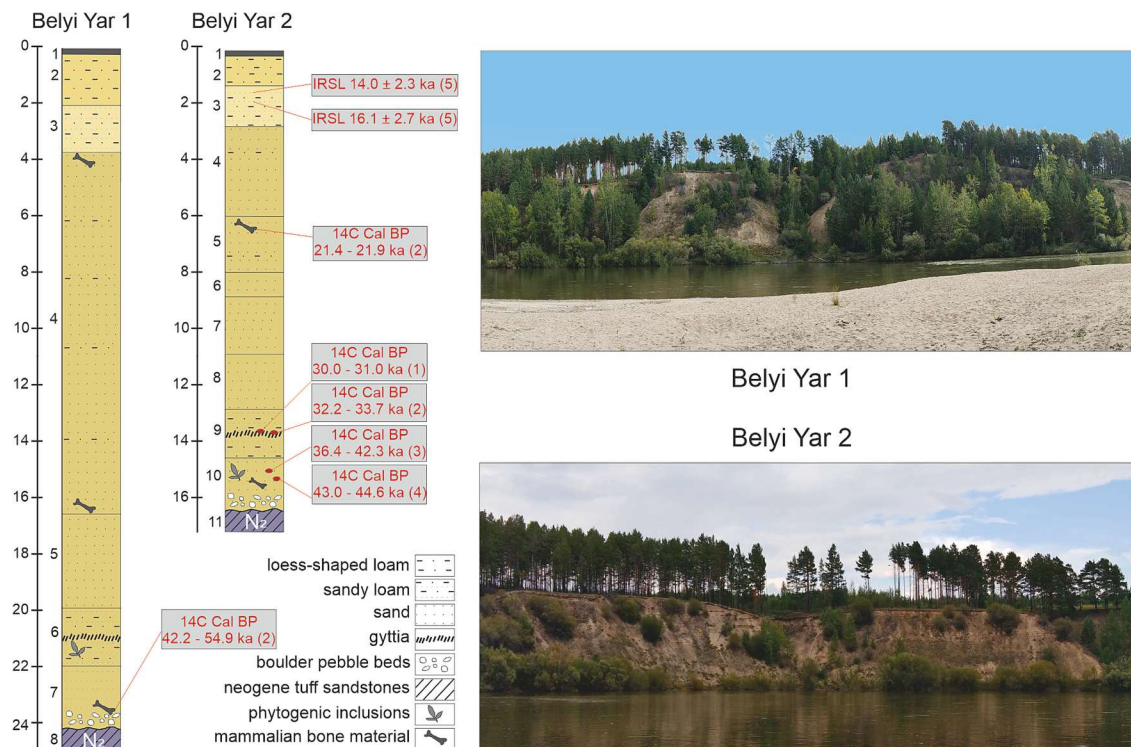


Fig. 7. Cross section and field photos of the Belyi Yar 1, 2 (after Shchetnikov et al., 2015). The dates are shown after: (1) Adamenko et al. (1975), (2) Shchetnikov et al. (2015), (3) Kul'chitsky et al. (1994), (4) Firsov et al. (1985), (5) Ufimtsev et al., 2003.

$\pm 2280$  (Ufimtsev et al., 1999).

### 3.3.2. Kyren Sand Field

Kyren Sand Field is located in the SW part of Tunka Depression. (Fig. 8, profile EF). This is a terrace-shape body lies at the foot of the northern slope of the Khamar-Daban Ridge. The sandy field from the north is limited by a 30-m escarp of the Irkut river meander. The section is represented fine-grained and silty sands with horizontal, oblique and inclined layering. Some layers have a turbulent texture. Mollusk shells and nodules of rounded clay forms (up to 5 cm) were found in the sediments, that excludes the aeolian origin of layered sands (Ufimtsev et al., 2002). The RTL-age of sand at a depth of 10 m is  $31,500 \pm 2,300$  (Ufimtsev et al., 2003).

### 3.3.3. Badary Sand Field

The largest Badar Sand Field (13x16 km) occupies the central part of the Tunka Depression (Fig. 8). It has a domed shape, towering over the floodplain of the Irkut River at a height of 40 to 150 m. There are no permanent watercourses and signs of waterlogging on the surface of the massif, there is only a small erosive network of ravines. From the east, BSF borders the area of the Koimorskaya lowland (Fig. 8). The Koimorskaya lowland and the Tunka River separated the BSF from the sandy strata covering the western slope of the Elovsky Spur (Belyi Yar Sand Field, Fig. 3). Engarga River and its lake-swamp lowland bound BSF in the west. To the north, the surface of the massif gradually decreases and passes into the lake-swamp valley of the Tunka River, which separates Badar from the piedmont of the Tunka Ridge. On the southern side, the slope of the massif is represented by a steep scarp with a height of 40 to 80 m, formed by a lateral washout of the Irkut River.

The thickness of Pleistocene sands recorded in wells drilled through the Badar massif reaches 400–500 m (Tectonics..., 1973; Vogt et al., 1998; Vogt and Vogt, 2007), and the maximum thickness coincides with the axis of the subsidence Tunka Depression. However, the thickness of the geomorphological structure of the BSF has not been estimated yet, since the depth of its base is unknown. Layers of the peat were found in the core from well D7 (Logachev 1958) (Fig. 8) at the depth of 150–180 m. This kind of peat is characteristic of shallow tundra reservoirs (Martinson, 1948; Logachev, 1958). This unit may be the lower limit of the BSF. The Badar Sand Field is composed of subhorizontal thin-layered

fine and medium-grained (average particle size from 0.12 to 0.35 mm) psammites with lenticular interlayers of coarse-grained sand and rare inclusions of fine gravel (Osadchy, 1995; Kolomiets, 2019). Various types of inclined, wavy stratification characterize the deposits. According to the mineral composition, these are polymictic, mainly feldspar-quartz sands with accessory minerals. According to mineralogical analysis (Ufimtsev et al., 2002), there is a slight excess of stable minerals for BSF sands, which may indicate a long-distance relocation.

In the article (Osadchy, 1995), sand deposits are characterised as clay-silt-sandy formations with a ribbon layering, in which underwater landslide structures are well expressed. The sediments contain aquatic malacofauna and diatoms (8 aquatic and 2 terrestrial species) in the upper part of the Badar section (Adamenko et al., 1975). The upper part of the sediments is composed of non-layered aeolian facies of fine-grained sands and sandy loams. The Badar Sand Field surface is covered with dunes. The age of the sands was preliminarily determined by TL and IRSL methods and amounted to  $65,200 \pm 4,000$  for the upper part of the layered thickness and  $12,420 \pm 2830$  (TL) and  $13,500 \pm 1820$  (IRSL) for aeolian sands (a sample from a depth of 1.5 m) (Ufimtsev et al., 1999, 2003). Luminescent dating shows the time of formation of aeolian deposits in the period from about 16.1 ka to 10.3 ka (Vogt et al., 1998).

## 4. Material and methods

We used remote sensing methods, as well as field study of sections and geochronological dating of sedimentary strata to solve the tasks set. In geomorphological mapping, we based on the interpretation of remote sensing data (SRTM with a resolution of 90 m, ALOS with a resolution of 30 m, TanDEM-X DEM with a resolution of 12 m). The analysis was carried out using Google Earth Pro, Global Mapper programs, with the construction of high-resolution 3D terrain models. Topographic maps (1:100,000 scale topographic maps), satellite images and published age data of some geomorphological objects on the TBs were also used (Chebotarev et al., 2021; Arzhannikova et al., 2020; Makarov et al., 2016; Chipizubov et al., 2003; Ritz et al., 2018). A comprehensive analysis of the elements of morphology, genesis and age of the terrace deposits, mapping of the complex of river terraces was carried out. We used the sedimentological method in the analysis of sediments in sections to reconstruct sedimentation environments and determine the

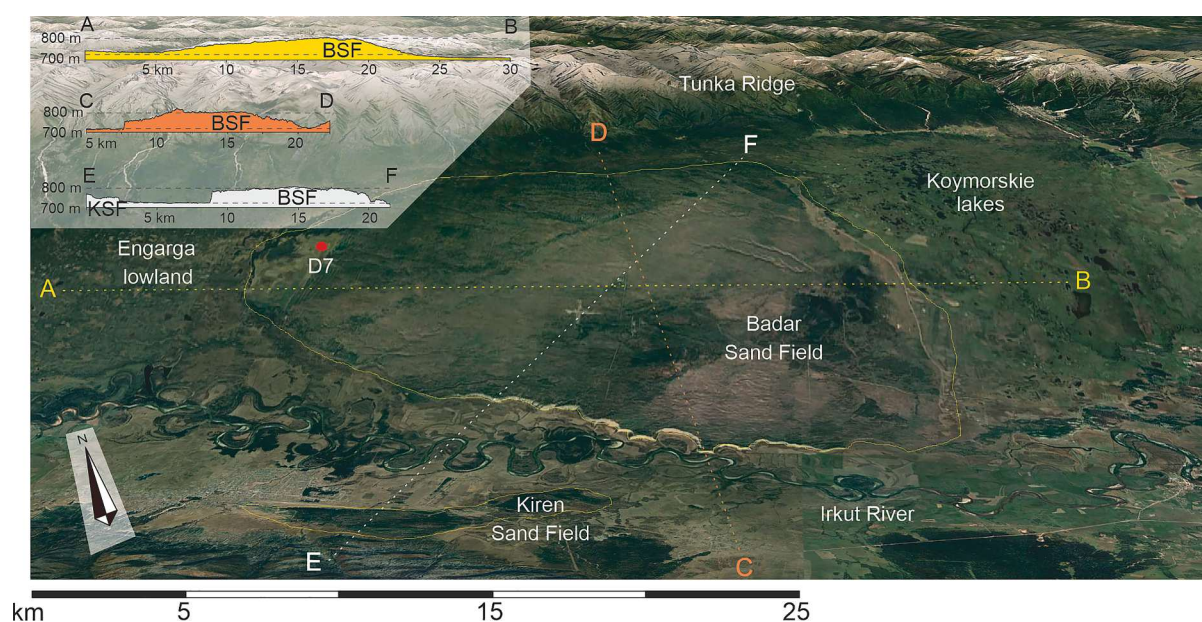


Fig. 8. Satellite image shows morphology BSF and KSF. View from the south. Location of profiles A-B, C-D, E-F. The red circle indicates the borehole - D7. (For interpretation of the references to color in this figure legend, the reader is referred to the web version of this article.)

genesis of sediments. The method includes field clearing, documentation, identification of general patterns of sedimentation and lithogenesis, identification of cyclical sedimentation processes of various ranks, determination of conditions for the formation of breaks in sedimentation, typification of sedimentation environments. To complete the picture, we also used published data on sedimentological analysis (Logachev, 1968; Ravsky et al., 1964; Adamenko et al., 1975; Kulchitsky et al., 1994; Kolomiets, 1998, 2019; Semenyev et al., 2014). We used OSL (post-IR IRSL) and  $^{14}\text{C}$  analysis for geochronological dating of sediments. Where sediments did not contain organic material suitable for  $^{14}\text{C}$  dating, the optically stimulated luminescence (OSL) method was used. Sampling was carried out using accepted methods with precautions against exposure of the sample to light. Sample preparation was conducted at the Luminescence Dating Laboratory of MSU/IGRAS (Kurbanov et al., 2019). Samples were first wet-sieved to give the grain size fraction 180–250  $\mu\text{m}$ , after which they were treated with 10% solutions of HCl, H<sub>2</sub>O<sub>2</sub> and HF. Separation of quartz and K-feldspar was carried out using an aqueous solution of sodium polytungstate ( $\rho = 2.58 \text{ g/cm}^3$ ). Then the quartz-rich fraction was treated with concentrated HF to etch the grain surfaces, and remove any remaining feldspar (Murray et al., 2021). Luminescence measurements were carried out at the Nordic Laboratory for Luminescence Dating (Aarhus University and Technical University of Denmark, Denmark) using Risø TL/OSL readers model TL-DA 15 and 20. Each reader is equipped with a calibrated  $^{90}\text{Sr}/^{90}\text{Y}$  beta source, with a known dose rate. In our case, quartz showed lack of sensitivity, so we obtained dates using K-feldspar. Stimulation was performed with an infrared light source; measurements were obtained according using a post IR IR SAR protocol, giving two IR stimulated signals, one stimulated with the sample at 50 °C (IR50) and the other at 290 °C (PIRIR290) (Thiel et al., 2011).

A standard dose recovery test (Murray, 1996) on five K-feldspars samples (six aliquots per sample) gave a ratio of  $0.95 \pm 0.05$  ( $n = 15$ ). The natural signal was first reset in a solar simulator (Hönle SOL 2) for 48 h. For each sample, three aliquots were used to determine any residual dose, and 3 aliquots were given a known dose similar to the natural dose. After residual subtraction, the average PIRIR290 dose recovery ratio was  $1.03 \pm 0.04$  ( $n = 14$ ). These procedures showed that our chosen measurement protocol is sufficiently able to accurately determine a known laboratory dose administered before any laboratory heating. No correction for anomalous fading was attempted for the PIRIR290 signal (Buylaert et al., 2012).

External dose rates were measured with a high-purity germanium detector for  $\sim 24$  h, following the procedures of Murray et al. (1987, 2018) and conversion factors given by Guérin et al. (2011). All samples were first pulverized and homogenized, then ignited at 450 °C for 24 h to remove organic material and cast in wax in a cup-shaped mould and left for  $> 3$  weeks to achieve  $^{222}\text{Rn}$  equilibrium. Cosmic ray contributions were calculated following Prescott and Hutton (1994). Internal dose rates to feldspar grains assumed a K concentration of 12.5% (Huntley and Baril, 1997). Measured saturation water contents were 25%.

To determine the age of organic material, we used the  $^{14}\text{C}$  method (Wagner, 1998). The accelerator mass spectrometer (AMS)  $^{14}\text{C}$  analyses were performed at the UMS INP SB RAS.

We used some features of the ichnological method to determine the conditions of sedimentation of BSF. The method uses ichnofossils as the results of behavior of benthic organisms. Traces are an in situ indicator of the paleohydrological regime and climatic conditions, the rate of accumulation of sediments and changes in the conditions of their formation (Buatois and Mangano, 2011). We used the interpretation of trace fossils to determine the paleoichnological facies, which gives an idea of the genesis of sediments.

## 5. Results

### 5.1. Sedimentation features and OSL dating of the Badar Sand Field

We dug up a geological section on the slope of the BSF to determine the age and genesis of deposits. The height of the scarp in this place is 40 m (cross-section is 39 m) above the level of the floodplain of the Irkut River (Fig. 9).

We have identified several sets of rhythmically accumulated sand deposits in the cross-section (Fig. 10). Most sets (2, 3, 5 and 6) are a repeating cycle of sedimentation from horizontally layered deposits at the bottom of the cycle to obliquely layered at the top (Fig. 11). The border between the different sets is contrasting, sometimes with erosion. The upper part of the sediments (set 1), represented by layers 10–60, has a horizontal occurrence and differs from the underlying sets, as well as groups 4 and 7. The total depth of the uncovered section was 39 m, however, the nature of the occurrence of the sediments in lower part of the section indicates that they represent the upper part of the previous sedimentation cycle, and not the lower boundary of the BSF.

The description is given along the section northern wall from top to bottom (Fig. 10).

#### 5.1.1. Set 1

This set includes a modern sod-soil layer (10), a layer of humus sandy loam (20), fine-grained gray (30) and yellowish (40) sand, non-layered sand (50) and a layer of obliquely inclined layered sands (60). The angles of inclination varies from 10° in the upper part to horizontal in the underside of the layer. In sandy layers 20, 30 there is a weakly expressed horizontal layering due to a change in the granulometric composition. Basically, the layers are composed of medium- and fine-grained poly-mictic sands. Layers 40, 50 are coarse-grained sand. Wedge-shaped structures deforming the boundaries (20, 30, and 40), bioturbations, and inclusions of grass and tree roots, moles are fixed in the layers. The lower boundary of the set is expressed by discordance. It cuts off the top of the underlying obliquely layered deposits. The total thickness of the



Fig. 9. The field photographs show the location of the geological cross-section on the erosional slope of BSF. A - View from the east toward the BSF slope and part of the Irkut Valley (beginning of dig). B - The cross-section and the bend in the relief (emphasized by vegetation). View from the south (the final part of the study).

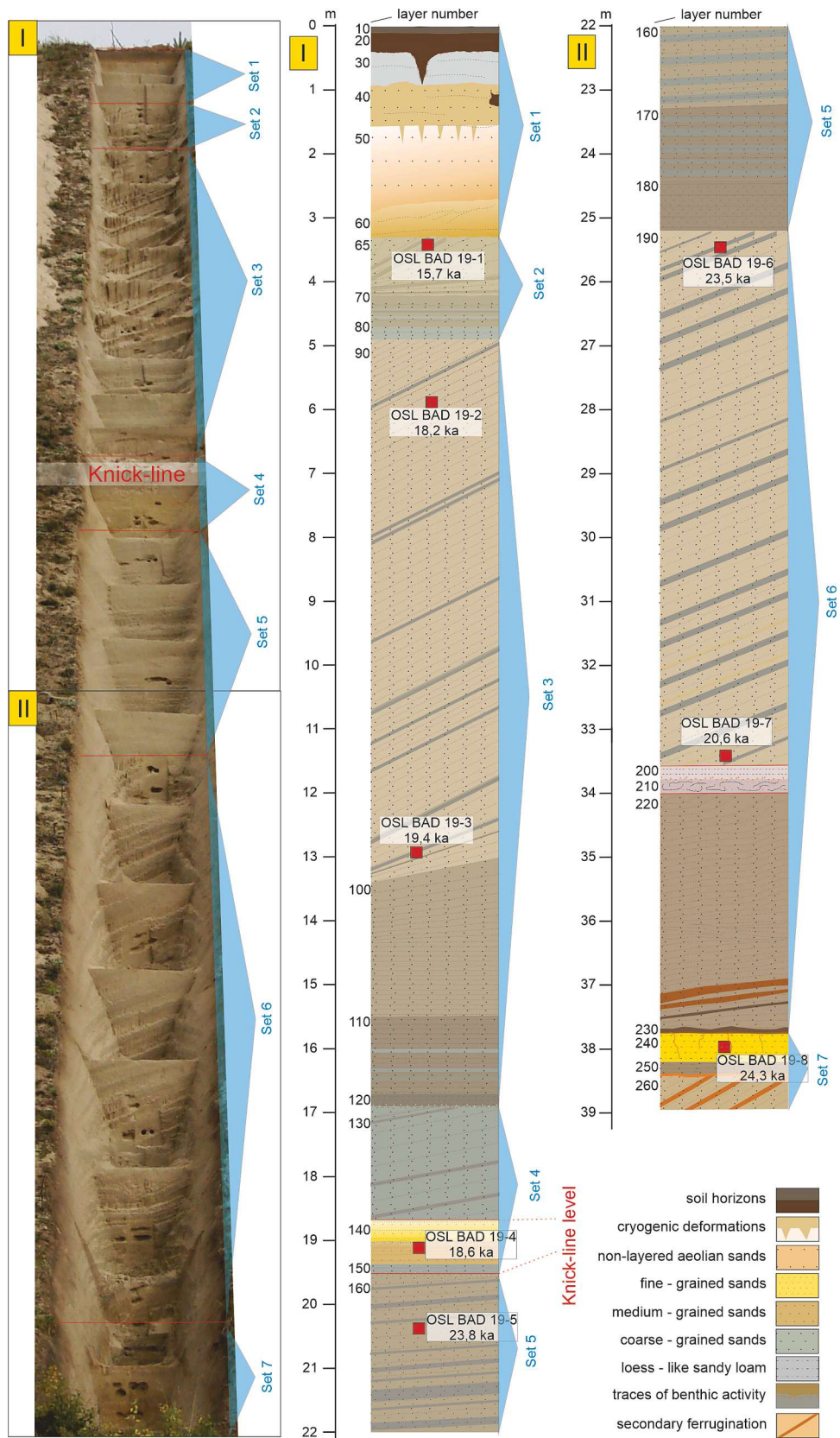


Fig. 10. The field photograph reflects the section of the BSF. A stratigraphic scheme of the Badary section is given. The red squares shows the sampling location and the OSL date. (For interpretation of the references to color in this figure legend, the reader is referred to the web version of this article.)



Fig. 11. A - Deposits of Set 1. B. Boundaries between Set 1/2 and Set 2/3.

set 1 sediments is 3.30 m. We interpret the origin of this set as subaerial.

#### 5.1.2. Set 2

The layering of fine, medium and coarse-grained sands (65, 70 and 80) represents the set. The layers of fine-grained sand are denser and wetter. In the lower part of the series, a layer of fine-grained sand with a horizontal layering prevails, gradually turning into an oblique layering with an inclination of up to 25° in the upper part. The thickness of fine-grained sand layers does not exceed 2 cm. Elongated micro-burrows are observed at the contacts of fine-grained sand layers. They distribute the layer material vertically and have rounded horizontal (up to 1 cm in diameter) and cylindrical vertical profiles (2–3 cm). Micro-burrows are filled with the material of the host matrix. The walls of the burrows have a high density due to carbonation. An extensive network of burrows forms a pattern of biogenic texture. We interpret this as traces of benthic communities' activity. (Fig. 12). The total thickness of the 2-nd set deposits is 1.8 m.

#### 5.1.3. Set 3

The layering of fine, medium and coarse-grained sands (90, 100, 110 and 120) represents the set. The layers can be divided into thin stuff up to 0.5 cm thick. In the lower part, the thickest fine-grained layers are up to 20 cm thick. The proportion of coarse-grained sands increases up to 20 cm the section, and fine-grained - decreases to three cm. Contact with the overlying sediments is clear. The total thickness of the 3-rd section is about 12 m.

#### 5.1.4. Set 4

There are two formations of different genesis (130 and 140, 150) in this set. In the upper part (130), these are light gray medium and coarse-grained sands, with uniform parallel oblique layering, sorted and well washed. This formation lies with discordance on layer 140, divided by color and granulometric composition into 2 parts: the upper one is lighter and drier. It is separated from the lower, darker, moist and dense by a small stuff with wavy layering (up to 10 cm of thickness). Layer 140 is underlain by sub-parallel layers of coarse-grained sand (150), light gray in color, up to 20 cm thick, which overlap set 5 with dissolution. At the height of this section, the horizontal bend (knick-line) stretched along the entire length of the slope, is fixed in the relief. The bend exists due to the denser structure of set four and its greater resistance to erosion (Fig. 9).

#### 5.1.5. Set 5

There is a layering of wet fine-grained and dry medium-grained sand with the inclusion of coarse-grained sand layers (160, 170 and 180) in this set. Layers of fine-grained sand up to 10 cm thick dominate the lower part of the set. In the upper part – layers of medium-grained sand with a thickness of up to 10 cm. A thin layer of up to 0.5 cm is clearly visible inside each layer. The upper boundary of the layer is washed and overlain by horizontal sediments 150. Set five lies on the sediments of set six with dissolution.

#### 5.1.6. Set 6

Alternating layers of fine and medium-grained sand (190, 200, 210,



Fig. 12. The photo shows a biogenic texture of sediments. Traces of paleoichnofauna (borrowing and bioeroding activities).

220 and 230) represent this set. Layers with a large number of fine-grained gray interlayers (containing dark-colored minerals) and a small number of medium-grained yellow interlayers predominate in the lower part of the set. The gray layers are wetter and denser. Higher along the set, the thickness of medium-grained yellow layers increases and the thickness of fine-grained gray layers decreases. A thin layering is visible inside each layer, due to a change in color and grain size. The layering is parallel in the lower part of the set (the bottom of the layer 220), then gradually turns into a gently undulating, concave (in the middle and upper part 220) and oblique (190). The angle of the layers inclination in the upper part is close to 30°. At a depth of 33.6 m, there is a layer of horizontal coarse and medium-grained sands with unclear boundaries (layers 200 and 210). Layer 210 has traces of turbulent eddies. At the bottom of the set, there is a layer of coarse-grained sand with the inclusion of a large number of micaceous minerals with traces of ferruginization. Set six ends at a depth of 37.7 m.

### 5.1.7. Set 7

This set includes 240, 250 and 260 layers, the formation of which correlates with different conditions. Layer 240 consists of fine sands and sandy loams. The deposits are yellow, very dense, with traces of ferruginization. The sand is not washed, with a large number of dusty particles. The physical parameters of the sediments of this layer show its subaerial genesis. There are pseudomorphs along the roots of plants, which is typical for soils. Layered washed sands with ferruginization in the lower part represent layer 250. Layer 260 consists of obliquely layered medium-grained, washed sands with an angle of incidence of the layers up to 40°. Ferruginization is visible from the contacts of the inclined layers. These layers represent the final stage of the formation of the previous set.

It should be noted that an extensive network of bioturbations (bio-print) occurs in the section at all depths. This represents traces of vital activity (burrowing and bioeroding) of paleoichnofauna belonging to benthic organisms. We observe a clear ichnotexture of sediments, which is expressed by numerous intergenic traces of benthic activity inside the layer or at the boundary between layers, in horizontal and vertical projections (Fig. 12B). This distinguishes them from injection textures, crumpling deposits, syneresis cracks, etc.

To estimate the age of the sands, the method of direct OSL-dating of sand by feldspar was applied. We took samples along the profile of the section in order to characterize the age of the sediments of each sedimentation cycle. We excluded from the assessment only the upper part of the aeolian section, for which the age is  $12420 \pm 2830$  (TL) and  $13500 \pm 1820$  (IRSL) (Ufimtsev et al., 1999, 2003; Vogt et al., 1998). As can be seen from the table, the dates obtained were arranged in a linear sequence from 24.3 to 15.7 ka with slight deviations in 3, 5 and 7 samples.

Below are the OSL dating results of samples by feldspar, conducted at the Aarhus University, Denmark (Table 1).

## 5.2. Zaktui pit

We have also carried out research on the slope of the Khamar-Daban Ridge and within the modern valley of the Irkut River to obtain additional data on the nature of sediments in the peripheral parts of the Tunka Depression.

The pit was excavated on the Khamar-Daban ridge slope (760 m asl), which is located at the southern side of the Tunka Depression (Figs. 3, 13).

Description of the northern wall:

- (1) Modern plowing layer. The lower border of the layer is uneven. Thickness 0.22–0.3 m.
- (2) A yellowish sandy loam layer with the inclusion of grains of coarse uncoated sand with a large number of dusty fractions and thin layers of brown loam. Thickness from 0.07 to 0.20 m.

**Table 1**  
OSL ages for samples the Badary Sand Field.

Sample	Lab code	Object	Depth (m)	Water content (%)	Age (ka)
BAD-19-1	208,688	K-feldspar	3.35	25	15,7 ± 1,3
BAD-19-2	208,689	K-feldspar	5.90	25	18,2 ± 1,2
BAD-19-3	208,690	K-feldspar	12.85	25	19,4 ± 1,4
BAD-19-4	208,691	K-feldspar	19.10	25	18,6 ± 1,7
BAD-19-5	208,692	K-feldspar	20.35	25	23,8 ± 2,1
BAD-19-6	208,693	K-feldspar	25.45	25	23,5 ± 1,2
BAD-19-7	208,694	K-feldspar	33.45	25	20,6 ± 1,6
BAD-19-8	208,695	K-feldspar	38.00	25	24,3 ± 1,4

- (3) A layer of overlapping red-brown clays with yellowish sandy loams and lenses of fine-grained uncoated sands. In the lower part of the layer, there are lenses of gray carbonated sandy loams with a thin layering. A large amount of mica, a single gruss 0.4–0.45 m.
- (4) A set of overlapping thin-layered sandy loams. The thickness of the layers is 1 mm. The layering is caused by a change in color from dark gray to light gray.. Sandy loams contain sand layers. The sand is dusty, uncoated, from fine to medium-grained, light gray in color. The layer is broken by cracks with an offset of up to 4 cm (strike). Re-deposited weathering products on granites represent the sand lenses. The eastern crack in the lower part is filled with the same sand. The lower border of the set is marked with a red color (ferruginization).
- (5) This sandy light gray layer with numerous of granite gruss is a product of the re-deposition of weathering crust on granites. It contains wavy layers of fine-grained sand and layers of gray loam filled with granite gruss.
- (6) The set is represented by coarse-grained quartz sand. There is a layering, emphasized by secondary ferruginization. The thickness of the layers is about 1 cm. The sediment is a recomposed product of granite destruction. The sand is washed, there are no dusty particles. Mica is in single copies.

Layers 4 and 5 can be interpreted as deposits of the aquatic environment. The height of these layers of 763 m asl coincides with the upper level of the layered sands of the BSF. In the section, these thin, well-stratified layers are interspersed with deposits of unsorted proluvium. This indicates the conditions of the coastal zone of a low-flow reservoir with an unstable water level. The accumulation of fine-grained sediments in the aquatic environment alternated with the arrival of larger detrital sediments from temporary watercourses, which eroded the slopes when the water level in the paleolake decreased.

## 5.3. Landslides and rockfalls in the Irkut river valley

The existence of BSF with a volume of  $\sim 16 \text{ km}^3$ , an aquatic genesis of deposits, suggests that their formation could occur in a large lake. The size of the reservoir can be estimated on the parameters of the sand body and alluvial deposits it formed on the slopes of the Khamar-Daban Ridge. The shape, size and height of the BSF indicates that the level of the reservoir should not be lower than the upper level of its alluvial part. Excluding the upper level of aeolian sediments in the BSF (thickness 3 m) exposed by the section, the upper boundary of layered sands is 765 m asl. However, given the inconsistency of the boundary of obliquely layered lake-delta sands and overlapping horizontal subaerial sediments, it is obvious that the top of the aquatic sediments has undergone

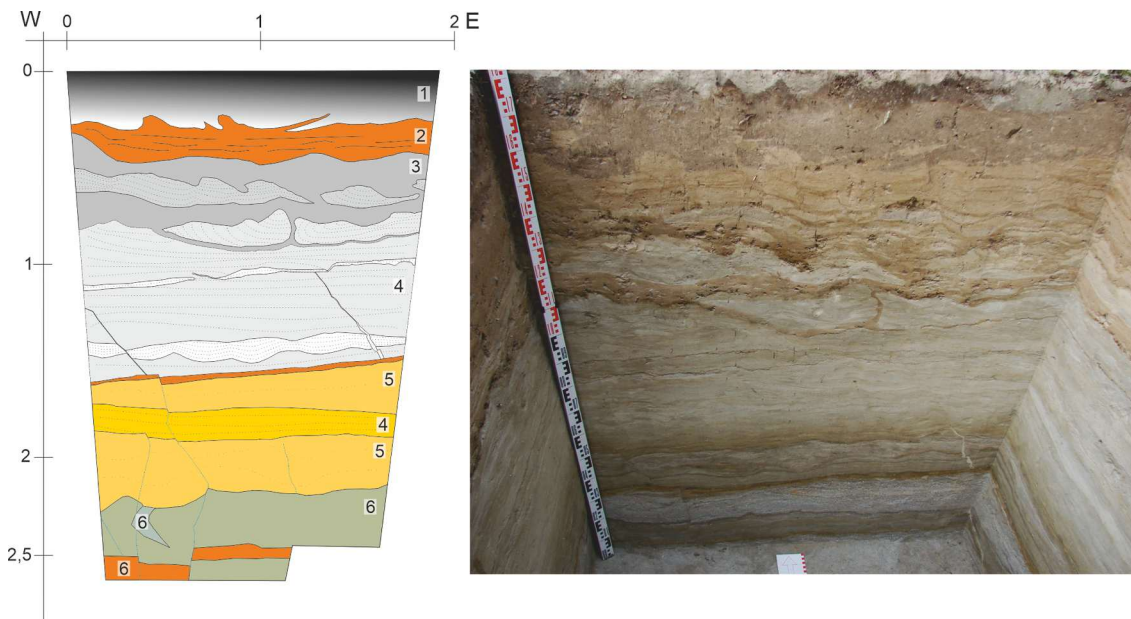


Fig. 13. Stratigraphic sketch of the deposits in the cross-section of the pit and a field photograph with a view of the northern wall.

aeolian erosion, and the level of 765 m above sea level is the minimum of the paleolake level.

We modeled a reservoir with such water level and got the probable location of the dam of the Irkut River. The Tunka Depression is bounded from the north and south by high mountain ridges and from the west and east by low-mountain spurs. The Irkut River drains the Tunka

Depression. In the Elovsky Spur, there is a single narrow outlet valley. (Fig. 1 C). This creates the geomorphological conditions for the formation of a dammed lake. Using satellite images and TanDEM-X data, we found fragments of landslides and rock fall in the narrow part of the valley (Fig. 14 A, B). This series of collapses and landslides, arranged sequentially, could represent a dam with a length of more than 4 km,

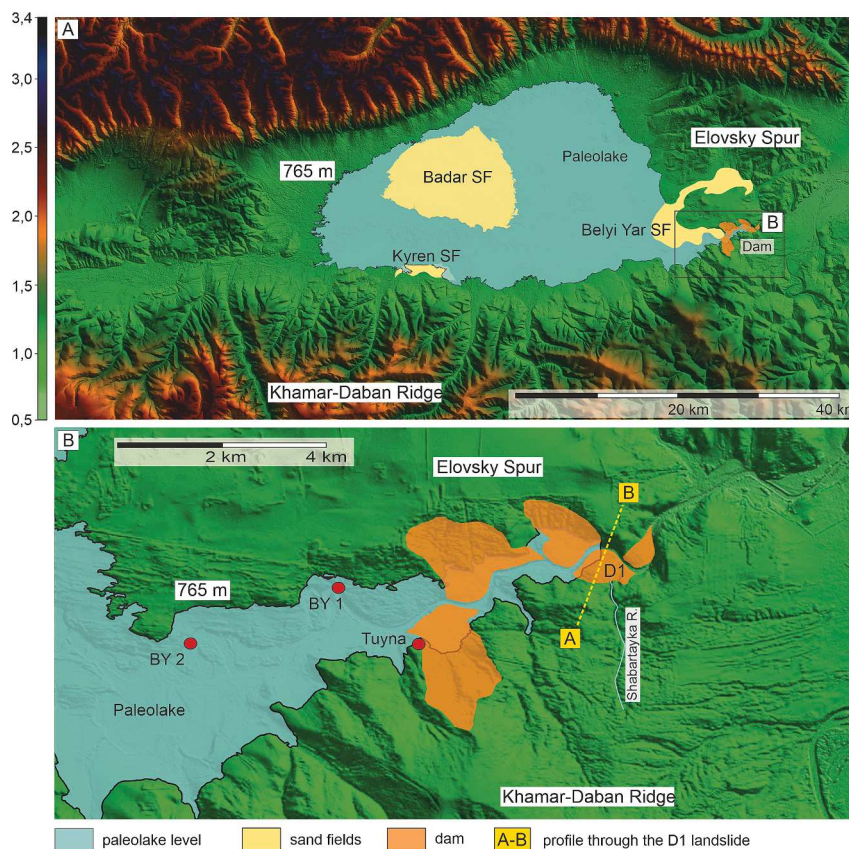


Fig. 14. A - Reconstruction of a paleolake with a water level of 765 m asl. B - A detailed scheme of the Irkut River dam location in the Elovsky Spur. Red circles mark the places of the sections of the Belyi Yar I, II, Tuyna. (For interpretation of the references to color in this figure legend, the reader is referred to the web version of this article.)

locking the valley of the Irkut River, which is the only channel of runoff from the Tunka Depression.

The most probable cause of gravitational shifts is the loss of stability of the slope due to the rapid antecedent incision of the Irkut River into the Elovsky Spur rising as a result of uplift (Shchetnikov and Ufimtsev, 2004; Ufimtsev et al., 2009). The trigger mechanism of the slope collapse could be the strong paleoearthquakes. Paleoeearthquakes associated with faults, controlling the evolution of the TBs. Data on earthquakes with a magnitude of  $\sim 7.5$  for the late Pleistocene - Holocene were obtained from studies of paleoearthquakes in the Tunka, Main Sayan and Mondy fault zones (Chipizubov et al., 2003; Arzhannikova et al., 2004; Ritz et al., 2018; Arzhannikov et al., 2018; Arzhannikova et al., 2023). In addition to that, Khromovskikh (Seismotectonics... 1968) attributed all landslides in the bedrock of the Khamar-Daban Ridge to the group of seismo-gravitational displacements. In fact, a series of landslides concentrated on a small area indicates the similarity of conditions and their syngenetic origin. Each of these landslides could create a backwater. However, the largest landslide D1 (Fig. 14 B) could completely block the narrow valley of the Irkut River at this point to a considerable height. The landslide is located at the confluence with the Irkut River of its right tributary, the Shabartayka River (Fig. 14 B). The sliding plane and its upper point (880 m asl), located on the rocky promontory of the Khamar-Daban Ridge are clearly visible on the DEM. The landslide descends into the valley with a wide tongue, while its more mobile avalanche top part (Strom, 2022) could be thrown up on the opposite side of the Irkut Valley. Erosion scarps occur on the slope in the height range from 780 m asl to 820 m asl, which may be preserved fragments of the dam. The volume of displaced bedrock preserved to date is about 19 million  $m^3$  with a landslide area of 0.5  $km^2$ . The total volume of the landslide, including its eroded part, could be 35–40 million  $m^3$ , with an area of 0.8 – 1.0  $km^2$ .

The profiling data indicate that the maximum height of the dam, created by the landslide, could have reached 820 m asl (Fig. 15). Most of the Tunka Depression at this time was under water, during periods of maximum filling. However, in the paleolake modeling, the reference point was the maximum height of lake sediments in Badar section, which is 765 m asl.

The slope deformations and a strong sediment flooding are also observed in a wide tributary in the SE of Tunka Depression closure. It is located on the slope of the Khamar-Daban Ridge at its junction with the Elovsky Spur. We dug a pit in the western side of the valley that showed the presence of sandy alluvial deposits, peat and ribbon clays characteristic of conditions of low-flowing water or a drainless reservoir (Fig. 16 D). Thick lenses of discontinuous permafrost and ice are visible on the technical sections of the slope for the highway under construction (Fig. 16 B, C). With seasonal thawing of permafrost in the valley, a landslide is activated, the creep movement of which is recorded in the annual deformation of the roadway. The landslide is clearly visible on satellite images and DEM (Fig. 16A). This area is completely located in the zone of dammed lake.

#### 5.4. Study of floodplain and terrace deposits

We made a detailed investigation of the alluvial deposits of the floodplain and above-floodplain terraces of the Irkut River in Tunka Depression, to determine the sedimentation conditions, the age of the deposits and the nature of the river incision (Fig. 3). The cross-sections of alluvial deposits in the western part of the Tunka Depression (Shimki), central (Ibogai) and eastern (Zatunka) were studied (Fig. 17 A, B, C). The history of sedimentation was reconstructed using instrumental measurements of the terraces height, opening of the riverbank outcrops and dating  $^{14}C$  of samples. We present a general characteristic for all sections, bearing in mind that the formation of terrace deposits occurred under similar conditions and their structure is generally similar. Coarse-grained sands of channel alluvium with an obliquely layered structure, traces of intense ferrugination, interlayers with a high concentration of heavy minerals (magnetite) and the inclusion of gravelites were found in the lower part of all sections along the Irkut River in the Tunka Depression. Above the alluvium deposit, as a rule, sub-horizontal medium- and fine-grained stratified sands and sandy loams of channel, floodplain or oxbow facies occur unconformably. The bedding is thin, obliquely undulating and is associated with the formation of flow ripples.

Loamy layers with wood and charcoal are found in sections. In the Shimki section (Fig. 17 A), sediments of abandoned meander were found. Deposits of this generation are disturbed by cryogenic or seismogenic deformations of different amplitudes (possibly with the participation of both processes) in almost all sections. This level of sediments falls into the zone of the seasonal cycle of freezing-thawing. Widespread permafrost in the region (Bulmasov, 1963; Alexeev et al., 2014) as well as high seismic activity of the region (Larroque et al., 2001; Chipizubov et al., 2003; Arzhannikova et al., 2004; Ritz et al., 2018; Arzhannikov et al., 2018; Arzhannikova et al., 2023) predetermined deformations of the original structure and texture of sediments. Aeolian deposits of different thickness cover the deposits of this generation. They contain gray sandy loams and reddish fine-grained sands. In the section of the Zatunka-2 (Fig. 17 C), this layer is represented by dune sand, deformed by cryogenic or seismogenic processes.

In general, dune formations are widespread on Tunka Depression surfaces at different levels of relief (on the above-floodplain terraces, on the slopes of ridges bordering the basin, on the surface of BSF and Belyi Yar) due to the intensive moving of sandy sediments, which occurred at different stages of the Holocene up to the present. In the Zatunka-1 section dune sands with a thickness of up to 5 m are located on the surface of buried soil with an age of 523–662 cal years BP (Fig. 18).

Thus, Holocene sedimentation in the accumulative zone of Tunka Depression happened according to the scenario of the formation of perstrative alluvium in a wide meander field of the Irkut River. The formation of terraces scarps occurred due to lateral erosion during the migration of the riverbed with alternating deposits of river and floodplain facies. Measurements of the terraces height at observation points

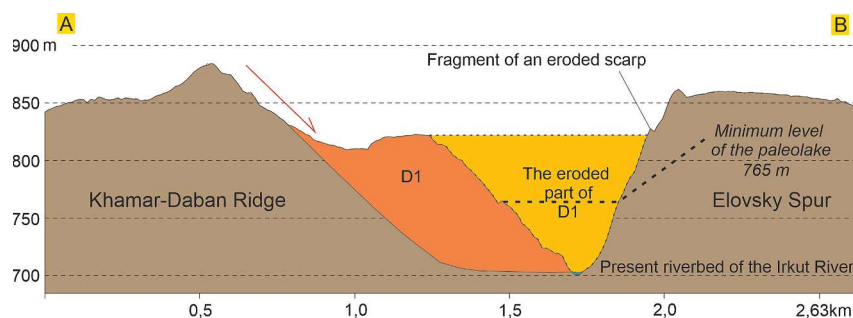


Fig. 15. Profile through the antecedent valley of the Irkut River and a large landslide D1 in the Elovsky Spur. The preserved landslide on the slope of the Khamar-Daban Ridge is marked in orange, its eroded part is colored in yellow. (For interpretation of the references to color in this figure legend, the reader is referred to the web version of this article.)



Fig. 16. A. DEM-model, demonstrates the valley in the SE part of the Tunka Depression deformed by a landslide. B. View of the valley from the east. The mound of earth-covered ice and local depressions associated with seasonal thawing are clearly visible. C. The lens of permafrost in the sediments. D. Inversion stratigraphy of the landslide sediments: the age of the soils at the lower part of the section is younger than the age of the peat covering the sands.

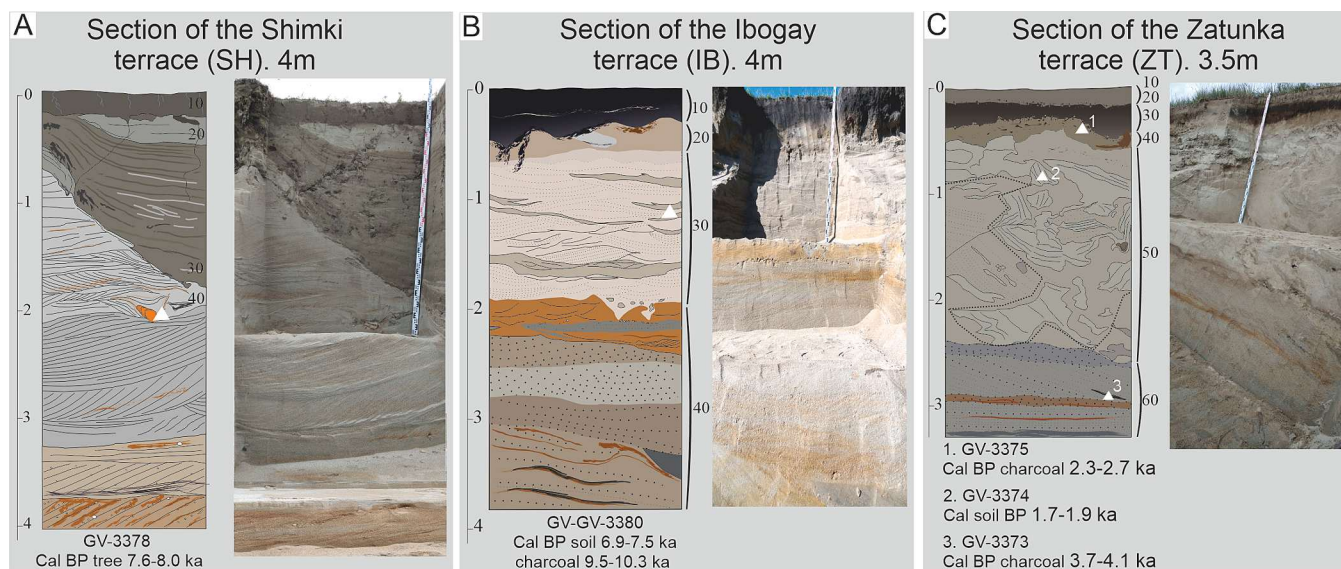


Fig. 17. Sections of the terraces of the Irkut River in the Tunka Depression (location on Fig. 2). The white triangles show the sampling points.

(Fig. 3) showed that the height of Holocene floodplain terraces ranges from 2 to 4 m along the entire length of the river within Tunka Depression. In some cases, pseudo-terrace ledges with higher surfaces

were observed. They are formed when the marginal parts of the river fans draining the Hamar-Daban Ridge or its piedmont turn out to be in the area of lateral erosion.

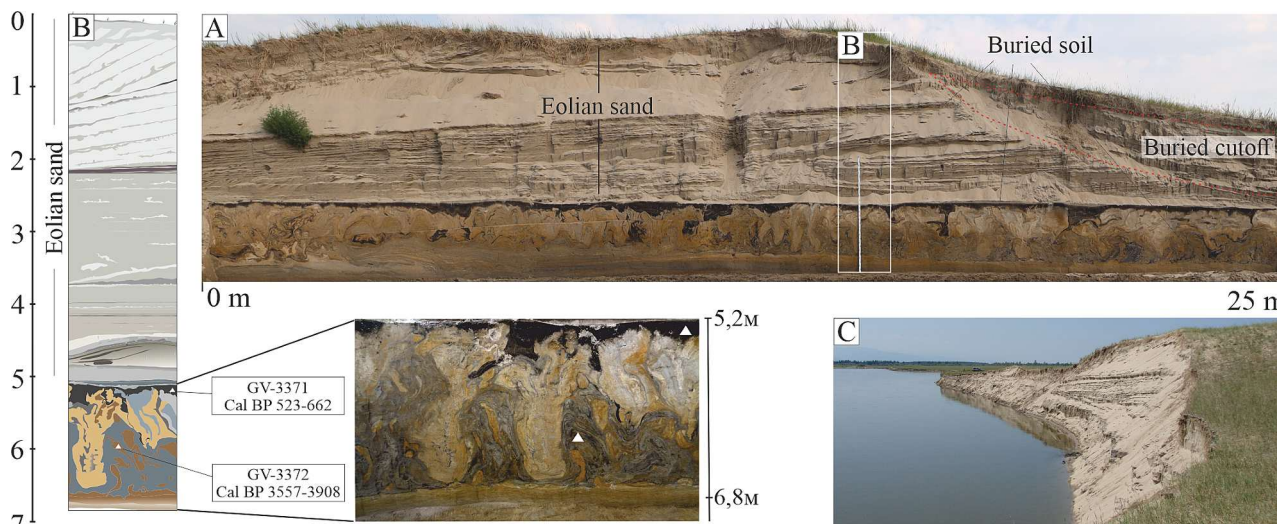


Fig. 18. A – Photo showing a general view of the cross-section Zatunka-1 located on the left bank of the Irkut River (point 7 on Fig. 2). B – Cross-section cleaned 2020 with dated <sup>14</sup>C soil samples. C - Photo showing the location of the studied section (buried terrace by dune sands on the left bank of the Irkut River). View of the site from the east.

The table below shows the main radiocarbon dating data known to date. Moreover, our new dates are included in the table. The age of the deposits of the above-floodplain terraces of the Irkut River in the sections estimated by us is within the limits of the Holocene.

Table 2. Published and new radiocarbon dating of deposits from terraces in the Irkut river valley within the Tunka basins.

6. Discussion

Summarizing the data on the genesis of Tunka Depression sand deposits, the most informative are the results of a comprehensive granulometric analysis (Kolomiets, 1994; 1998; 2010; 2019; 2021). The research showed that BSF deposits were formed in the aquatic environment under prolonged stable dynamic sedimentation conditions in the late Pleistocene. The parameters of the aquatic environment

reconstructed by Kolomiets (2019, 2021) are most consistent with the conditions of turbulent river and bottom currents of a large aquatic complex with seasonal fluctuations in water content. Facies and granulometric analysis data indicate that this complex combined limnic and alluvial sedimentation conditions with a shifted balance in the coastal facies of the lacustrine group (Kolomiets, 2021). Our research confirms this interpretation, however, leaving aside the author’s version of the “Baikal” origin of the reservoir. In our opinion, the entire complex of Tunka Depression sand deposits, represented by fragmentally preserved structures of Badar, Kyren and Belyi Yar could have been formed by a local, slow-flow dam reservoir enclosed in the boundaries of Tunka Depression. The bulk of sediments were brought into the depression by the Irkut river system (loose material from glacial and fluvio-glacial deposits of the Mondy and Ihe-Uhgun glaciers and glacial outwash plain (Fig. 1 C)), as well as rivers draining the Tunka and Hamar-Daban ridges.

Table 2  
Published and new radiocarbon dating of sediments within the Tunka Depression.

Lab code	Site	Sediments	Depth (m)	Samples	Data <sup>14</sup> C BP	Age Cal, BP	Reference
IGAN-3370	Belyi Yar 1	Gytia	22,5	Wood charcoal	44200 ± 4500	42177–54980	Shchetnikov et al., 2012
OxA-27618	Belyi Yar 2	Alluvial	10,0	Bone	17850 ± 90	21399–21984	Shchetnikov et al., 2015
SOAN-7290	Belyi Yar 2	Alluvial		Bone	28 730 ± 160	32254–33681	Shchetnikov et al., 2015
SOAN-577	Belyi Yar 2	Peat	13,4	Organic remains	26250 ± 300	30040–31038	Adamenko et al., 1975
SOAN-3144	Belyi Yar 2	Gytia	15,0	Organic remains	35440 ± 1860	36417–42498	Kul’chitsky et al., 1994
SOAN-141	Belyi Yar 2	Peat	15,8	Organic remains	40860 ± 480	43046–44551	Firsov et al.,1985
JIV-7420	Belyi Yar 2	Peat	15,8	Organic remains	38430 ± 1430	40680–44396	Maksimov et al., 2015
JIV-7361	Belyi Yar 2	Peat	15,6	Organic remains	38000 ± 850	41234–42954	Maksimov et al., 2015
UCIAMS 185968	Tuyna	buried soil	0,4	Organic remains	5475 ± 15	6275–6302	Berdnikov et al., 2017
KGM-Isa 170093	Tuyna	buried soil	0,7	Organic remains	6820 ± 40	7580–7724	Shchetnikov et al., 2019
KGM-Isa 170094	Tuyna	buried soil	2,4	Bone	32250 ± 190	36198–36981	Shchetnikov et al., 2019
UCIAMS 186319	Tuyna	buried soil		Bone	27,030 ± 270	30736–31690	Vasilyev et al., 2017
UCIAMS 186320	Tuyna	buried soil		Bone	47800 ± 3500	45198–54980	Vasilyev et al., 2017
OxA-25896	Tuyna	sandy soil	1,3	Bone	35900 ± 750	39636–42020	Kozyrev et al., 2014
GV-3378	Shimki	Alluvium	2,0	Organic remains	7043 ± 129	7617–8042	This paper
GV-3380	Ibogay	sandy soil	1,2	Soil	6339 ± 143	6931–7509	This paper
GV-3380	Ibogay	sandy soil	1,2	charcoal	8889 ± 171	9538–10305	This paper
GV-3371	Zatunka	sandy soil	5,2	Soil	592 ± 59	523–662	This paper
GV-3372	Zatunka	buried soil	6,0	Soil	3464 ± 73	3557–3908	This paper
GV-3375	Zatunka	sandy soil	0,4	charcoal	2450 ± 79	2350–2723	This paper
GV-3374	Zatunka	sandy soil	0,8	Soil	1885 ± 71	1691–1949	This paper
GV-3373	Zatunka	sandy soil	2,9	charcoal	3564 ± 78	3684–4086	This paper
GV-3383	Landslide	buried soil	0,8	Humus	21570 ± 230	25340–26338	This paper
GV-3383	Landslide	buried soil	0,9	Peatland	25670 ± 461	29,066–30,926	This paper
GV-3384	Landslide	buried soil	2,0	Organic remains	5954 ± 88	6558–7001	This paper

The Irkut River cutting through the Nilovsky Spur and leaving the antecedent valley into the wide Tunka Depression formed a voluminous sand deposit. In the inner field of Tunka Depression, due to the constant introduction of loose material, a delta sedimentary system was formed, which, as the basin was filled with water and sand, moved to the east, creating a complex three-dimensional delta body. Due to the relatively small balance of water intake during the ice age, the material managed to undergo primary sorting, forming rhythmic (varve type) sand deposits with different physical parameters (grain size, specific gravity of minerals, degree of processing, etc.). The differentiated energy of the sedimentation situation in the delta zone led to different degrees of sediment sorting, from good to very good. There are layers with deep differentiation of sand deposits by specific gravity, which leads to an increase in the concentration of heavy minerals (magnetite dominates) in dark layers formed, as a result, of wave-built activity or in the bottom traps zones. It is obvious that during periods of small water input the surface of the delta could be exposed to the erosive effects of subaerial agents. Thus, the deposits of the fourth and seventh sets of the Badar section (Fig. 10) have a significantly smaller size of the sand fraction and a pulverized loess-like structure. These sediments have accumulated in subaerial conditions and are indicators of the surface during periods of the reservoir water level changes. There is no fine fraction of siltstones in the Badar section expected for lake sediments. This indicates a relatively high flow energy, at which the fine suspension did not have time to settle and was carried away by the water flow. The aquatic sedimentation environment is also confirmed by the ferruginization of some layers, due to iron-containing minerals in the aquatic environment.

In our opinion, the change in the angle of inclination of sand deposits within each sedimentation cycle is associated with the peculiarities of the formation of different elements of the architecture of delta sediments. Slightly inclined or horizontal layers in the upper part of the cycle belong to the topsets phase (according to Gilbert, 1890; Scruton, 1955) of the above-water part of the delta, in which a subaerial component may be present. The main part of the delta is composed of steeply inclined (up to 30°) layers of the foresets phase, represented by a coarser material. In the lower part of the cycle subhorizontal deposits of the bottomsets phase are formed, lying parallel to the bottom of the reservoir. Monotonous sand cover in the delta front is characteristic of the “branching” delta type with constant migration of meandering channels forming the facies of the estuary bar. The material entering the delta is transported along the bottom of the basin according to this sediment distribution mechanism. Commonly this type of sediments demonstrates continuous series of changes in the size of fractions and in the angles of layers inclination (Reineck and Singh, 1980). The delta facies are characterized by traces of underwater landslide fixed (Osadchy, 1995). The almost complete absence of organic material at the entire depth of the section (the exception is an intermediate series of deposits between cycles three and four (knik-line, Fig. 10)) also indicates the continuous accumulation of sandy sediments in the aquatic environment. However, the presence of intermediate horizontal series deposits in the middle part of the section with a much smaller, silty fraction size and signs of aeolian genesis (set 4) indicates a temporary change in sedimentation conditions that falls on the time interval of 18–19 ka (sample BAD-19-4, OSL age 18.6 ka). A temporary change in the hydro balance and the withdrawal of the accumulated deposit in the Tunka Depression into the sphere of subaerial influence may be associated with a climate change at that time. Then, with the beginning of climate warming, the accumulation of sand masses resumed, which is reflected by the cyclic pattern - horizontal-oblique-subhorizontal sedimentation series from 3 to 1 (Fig. 10).

We consider the closure of the Tunka Depression drain in two stages as an alternative interpretation of subaerial layers interrupting delta sedimentation. The series of gravitational displacements observed in the antecedent valley (Fig. 14), blocking the exit of water from the basin, could be non-simultaneous. The recurrence of earthquakes with a magnitude of ~ 7–8 for the region in the Late Pleistocene – Holocene

was estimated as four ka (Ritz et al., 2018). A repeated gravitational collapse raising the previous level of the dam seems quite likely.

It is known, that despite the extreme conditions, the periglacial reservoirs were the habitat of invertebrates and some arthropod species, and traces of their vital activity are an effective tool for analyzing continental paleoecology. The repeated ichnofabrics that are present in the exposures are used to correlate sedimentation situations within sedimentary basins. According to the analysis of ichnofabrics, some parameters of the habitat of ancient benthic organisms are determined (Mikuláš and Dronov, 2006; Buatois and Mangano, 2011). In the section of the Badar sands, numerous traces of benthic activity are visible along its entire length, violating the integrity of stratigraphic levels by branched system of trails. In our case, the definition of ichnofossils to the species is not possible, but according to the classification schemes of benthic activity traces, sedimentation conditions are defined as Ichnofacies Skolithos, formed in the coastal conditions of a shallow reservoir. The predominantly vertical arrangement of cylindrical routes of burrowing organisms is characteristic precisely for turbulent shallow water conditions (Fig. 12 B) (Mikuláš and Dronov, 2006). This reflects the peculiarities of benthos adaptation to high-energy flow conditions. The predominance of vertical channels indicates a large content of organic particles that are suspended in a well-oxygenated water column by waves and currents (Buatois and Mangano, 2011; Howard and Frey, 1984; Anderson and Droser, 1998). The predominance of simple morphological traces of the same type of fossils is also characteristic of the facies of the coastal channel belt, sand bars. In pedogenized thin sediments of the floodplain, coastal sediments with active subaerial impact and deep bottom silty sediments, a significant diversity of ichnofauna usually observed, leaving a large number of species of trace structures.

Generally, there is no doubt about the question of the aquatic genesis of the Badar sands, when considering the entire complex of data obtained during its study. The issue of genetic similarity of the large sand complexes of Badar, Kyren and Belyi Yar is still unresolved. To assess the possibility of the formation of these sand structures at the same time and under the same conditions, it is necessary to confirm factually the existence of a reservoir within the boundaries of Tunka Depression in the range from 26 to 15 ka. To do this we have attracted additional research data (Zaktui prospect pit, landslide), described in the Results chapter. In 2019, the detailed research data on the geoarchaeological site of Tuyana, which geographically falls within our field of interest, was introduced into scientific circulation. We will present our analysis of these data in the context of studying the traces of the paleolake.

### 6.1. Correlation of the lake's existence time with a break in human settlement of Tuyana

The Tuyana archaeological site (51°42'49.12"N, 102°41'48.27"E) is located on the slope of the southern side of the Tunka Depression (Figs. 6, 19), at altitudes of 725 – 750 m asl, falling into the area of possible flooding by a dam reservoir. The distance from the object to the Belyi Yar – 2 is 1.5 km, to the BSF – 23 km. Ancient people inhabited the site in different periods of the Late Pleistocene – Holocene (AMC age of artifacts 6280, 7652, 35900, 36138, 49690 ka (MacEachern, et al., 2007; Shchetnikov et al., 2019)). However, the period we considered in the range from 25 to 15 ka is not characterized in the deposits of the archaeological site by traces of human habitation.

There was a break in human habitation on the territory of Tuyana from 31.071 ± 166 cal BP (UCLAMS 186319) (Shchetnikov et al., 2019) to 7652 ± 34 cal BP, according to 14C (KGM-Isa 170093) (Shchetnikov et al., 2019). In the section, this break is expressed by sandy loam deposits of unclear stratification lying with blurring on paleosoil with an age of MIS – 3 (Fig. 19) (Arzhannikova et al., 2020). Archaeologically, sandy loam layers are sterile. The species composition of the malacofauna from these deposits corresponds to the terrestrial hydrophilic swamp and wet meadow type (Shchetnikov et al., 2019). Based on the

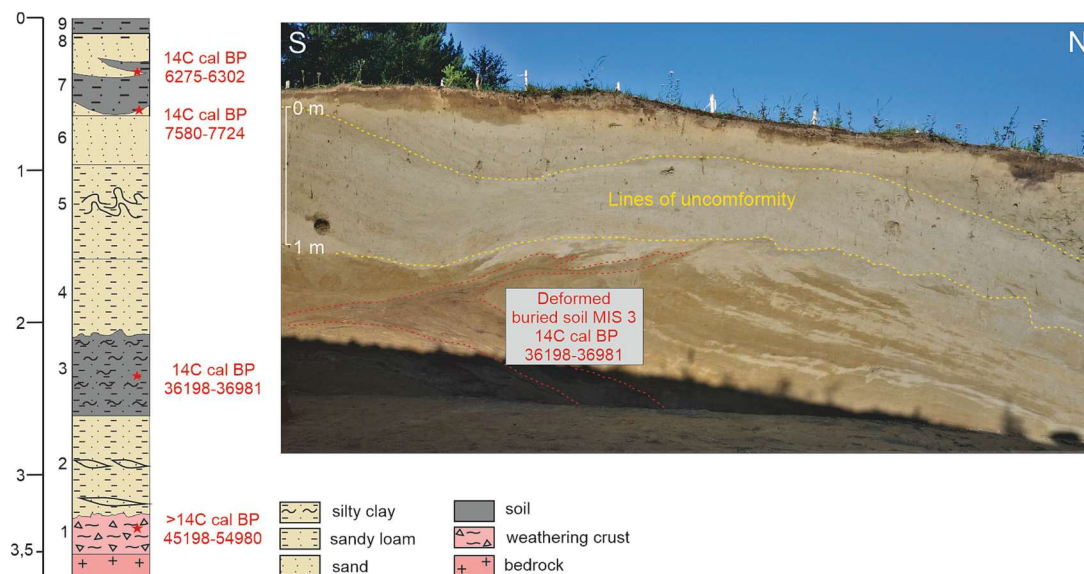


Fig. 19. Stratigraphic scheme of deposits of the archaeological site of Tuyana (after Shchetnikov et al., 2019; Arzhannikova et al., 2020) and a general view of the section. Radiocarbon ages according to (Shchetnikov et al., 2019). The yellow dashed lines show the zone of unconformity formed as a result of erosion in the Younger Dryas (Shchetnikov et al., 2019). (For interpretation of the references to color in this figure legend, the reader is referred to the web version of this article.)

results of magnetic analysis of the Tuyana sedimentary strata, it was concluded that the magnetic properties of the Tuyana section do not reflect the formation structure characteristic of the Siberian subaerial formation. Some data badly distinguish between modern soil and sand sediments. The composition of the magnetic fraction is the same throughout the section and is represented by magnetically soft minerals (magnetite/maghemite). This is not typical for the mechanism of formation of the “Siberian” magnetic properties and indicates an additional factor in the sedimentary process that equalizes the magnetic properties. Presumably, this is a ferromagnetic influx of material as a result of volcanic activity (Shchetnikov et al., 2019). However, the age of late Pleistocene episodes of volcanic activity in the region is ~ 13–14 ka, and the youngest episode dates to the age of ~ 1200 CE (Okinsky Plateau) (Arzhannikov et al., 2016). That is, the eruptions were after the formation of culture-containing deposits of Tuyana and sand massifs in the basin. In our version, the alignment of magnetic properties could occur due to the introduction of minerals from the lava covers of the Okinsky Plateau, the Khamar-Daban Ridge, the Nilovsky Spur by the Irkut River and the deposition of minerals in the conditions of the dammed lake in the Tunka Depression.

## 6.2. Levels of the paleolake

Summing up the known data on the Tunka Depression sand fields and the new data we have obtained on the Badar deposits and new sections in the periphery of the Tunka depression (Zaktui pit, Tuyana site, landslide), we get a picture of the existence of a giant sand massif of aquatic genesis in the late Pleistocene. Its upper level is fixed both within the sedimentation field of the Tunka Depression and on the slopes, in the height range from 720 to 820 m asl. A series of geomorphological formations (possibly of different ages), expressed by erosion ledges, was recorded at different heights of the western slope of the Elovsky Spur and the northern slope of the Hamar Daban Ridge (within Tunka Depression) during the analysis of the DEM and field studies. S. S. Osadchy (1995), being a proponent of the theory of the Late Pleistocene multi-lakes, believes that the existence of the reservoir is associated with the transgression of the waters of Lake Baikal into adjacent depressions during the period of maximum glaciation. However, the existed data (Arzhannikov et al., 2018; Arzhannikov et al., 2021a) indicate that the last high water level of Lake Baikal is not younger than 130 ka. At the

turn of the Middle and Late Pleistocene, the descent of ingressive waters from the Baikal Rift basins ended, which is confirmed by the formation of a complex of river terraces in the basins (Vyrkin and Opekunova, 2001; Ufimtsev et al., 2003; Opekunova and Kobylkin, 2009; Makarov et al., 2016). Published data about the age of the Tunka Depression sands and our new OSL dates of BSF sand deposits (Table 1) indicate their formation in the MIS 2 (Adamenko et al., 1975; Kul'chitsky et al., 1994; Ufimtsev et al., 2003; Vogt et al., 1998; Vogt and Vogt, 2007; Semenyev et al., 2014; Shchetnikov et al., 2015; Maksimov et al., 2020). Consequently, the age of the sands, as well as the absence of Baikal malacofauna in the sands, allows us to state the absence of a genetic connection of the sands from the sections of the Tunka Depression presented in this article with the Baikal transgression. We can assume local conditions for the formation of large sand massifs inside the depression as a result of the temporary standing of the paleo lake enclosed in the boundaries of Tunka Depression. We explain the absence of extended shorelines clearly expressed in the relief on the periphery of the basin, which were not found during detailed geomorphological mapping, by the unstable level of the paleolake, which did not allow coastal erosion objects to form. It may also happen due to seasonal fluctuations and the dependence of the water level of the paleolake on the climatic conditions of the periglacial zone. Here, the parameters of the water system are directly related to the state of the glacial covers, which are the source of water supply to the water area. Another factor that could affect the preservation of lake sediments and shorelines on the slopes of the Tunka Depression sides could be a complex of gravitational slope processes. Cryogenic processes in the form of slow creep displacements of watered loose sediments, which were recorded in all sections, were also complicated by the high seismicity of the region.

The version presented in this paper of the formation of the Tunka Depression sand massifs and, in general, the Late Pleistocene-Holocene relief of the inner field of the depression assumes two stages (Fig. 20). During the MIS-2 period, in the range of 25–15 ka BP, the formation of a dam reservoir occurred by blocking the antecedent valley of the Irkut River, which is the only channel of runoff from the Tunka Depression. The inner field of the depression (within the inner delta) was filled with lacustrine-alluvial deposits up to a level of 765 m asl as a result of the rise in the water level in the basin. This level is the possible minimum height of the dam in our model. It should be noted here that the thickness of the BSF is uneven, and to the northwest of our section, it exceeds

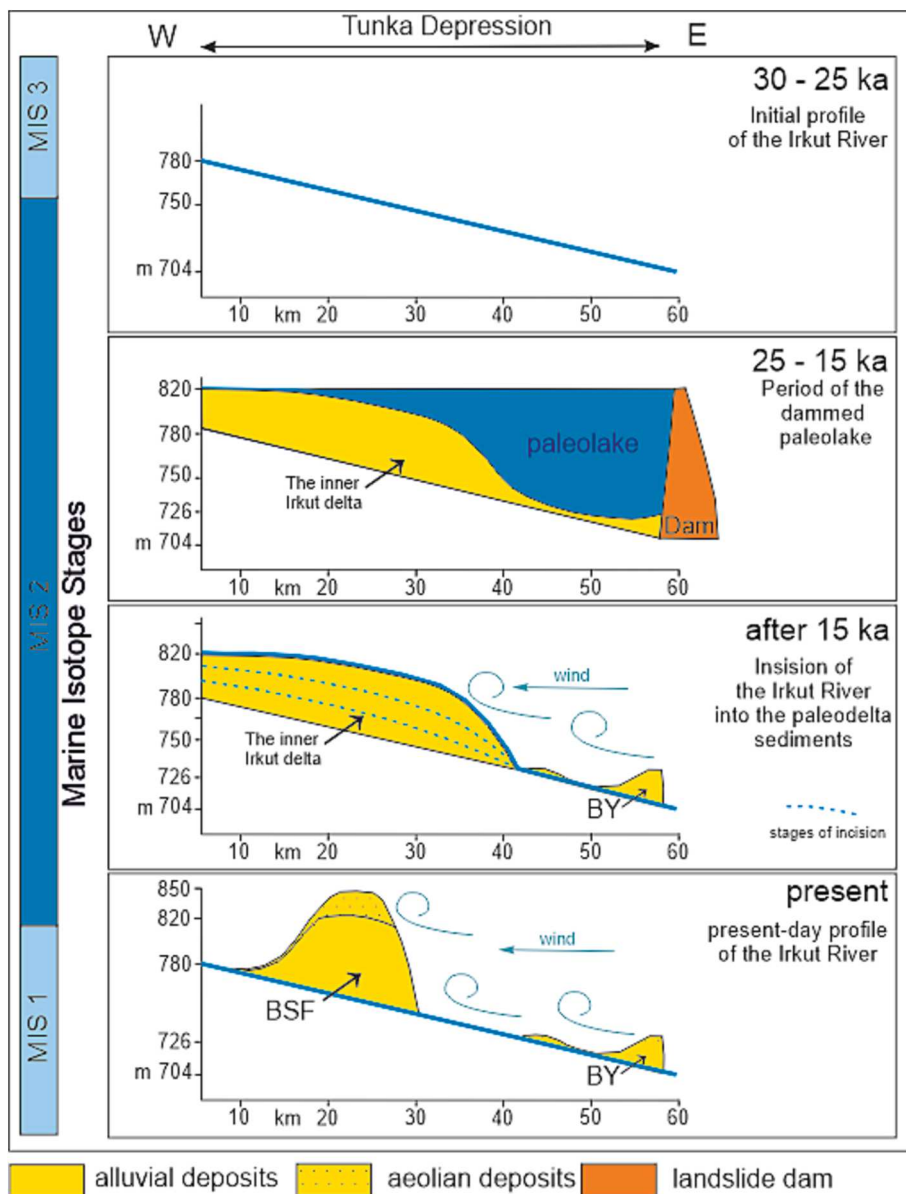


Fig. 20. Schemes of changes in the profile of the Irkut River over the past 30 thousand years within the boundaries of the Tunka Depression.

the modern surface of the depression by 130 m. We have no data on the nature of these deposits, most likely the upper part of the massif, above the 765 m mark, is composed of wind-blown sands, which is confirmed by the presence of a network of dunes and blowing basins on the BSF surface. However, if lacustrine-alluvial deposits spread higher than the level recorded in our section, this does not contradict our concept, since the maximum level of the dam could reach 820 m asl (Fig. 15). The descent of the reservoir was accompanied by deep erosion of accumulated sediments associated with the restoration of the natural river profile. A significant decrease in the lake level occurred at 15 ka. As a result, the surface of the inner delta emerged from the water and was reworked in top part by the aeolian process. Nevertheless, in places beyond the erosive impact of the Irkut River system, large sand masses have been preserved fragmentally. The age of the paleolake descent may be slightly younger, as the upper level of the delta sediments has been reduced by aeolian activity. This can be confirmed by the occurrence of alluvial sands in bottom deposits of Lake Engarga sediments (Fig. 6) with an age less than 14.8 ka. Further formation of the surface relief of the Tunka Depression is characteristic of rift basins. The formation of the upper cover of sediments in the Tunka Depression, represented by

variations of alluvium and overlapping aeolian sediments, was determined by climatic conditions in the Holocene time, as evidenced by our analysis of terraces of the Irkut River. There are no markers of the inversion tectonic component in the loose sediments of the Holocene inside the Tunka Depression. It is obvious that the basis of erosion of the Irkut River in the Late Pleistocene-Holocene time did not undergo significant changes. The studied sections of the terraces indicate descending tectonic movements in the basin, which is typical for rift regimes. This process was accompanied by the formation of both normal floodplain-terrace complexes and pseudo-terraces during lateral erosion of deluvial-proluvial slopes of piedmont and fans of lateral tributaries.

### 7. Conclusions

A comprehensive study and determination of the genesis and age of sand massifs in the Tunka Depression of the Baikal Rift Zone allowed paleogeographic and geomorphological reconstructions to be carried out. We have established that a dammed lake and then aeolian processes played the main role in the development of the sedimentary cover of the Tunka Depression in the Late Pleistocene-Holocene. We obtained data

on the aquatic conditions of the Badar Sand Field sedimentation. The Badar section with a rhythmic structure reflects the dynamics of the formation of the inner delta in conditions of weak currents complicated by seasonal fluctuations in the water level. The OSL dates of the entire section reflect the time interval of 24–15 ka during which the accumulation of the main part of the sands occurred.

Two sequences of sediments reflecting the dynamics of sedimentation are distinguished in the section. The lower main block is represented by a deltaic alluvium of a sandy fraction formed in conditions of a low-flowing reservoir. Aeolian sandy deposits, the formation of which occurred after the drainage of the reservoir, represent the upper part of the section.

The formation of the paleolake within the Tunka Depression is associated with the large collapses and landslides, which blocked the Irkut river valley in the Elovsky Spur. Using the geomorphological reconstruction, we have established the maximum height of the dam at 100–120 m. The analysis of the terraces levels, the sections and  $^{14}\text{C}$  dating in the Irkut river valley showed the absence of tectonic markers of inversion within the Tunka Depression in the Holocene. Unlike the marginal depressions of the TBs, Tunka Depression continues to subside. This does not contradict the transpressional stress field with a north-eastern compression axis, which has prevailed in this region since the late Pleistocene. In this regime, local extension occurs along the northeast-trending segment of the Tunka Fault, which controls the development of the Tunka depression. Thus, the 40–90 m incision of the Irkut River into the BSF did not occur as a result of uplift, as previously assumed (Ufimtsev et al., 2009; Shchetnikov, 2017). The main reason for the incision was the restoration of the equilibrium of the longitudinal profile of the river due to changes in sedimentation conditions in post-glacial time.

#### CRediT authorship contribution statement

**A.A. Chebotarev:** Conceptualization, Writing – original draft, Investigation. **S.G. Arzhannikov:** Methodology, Supervision, Validation. **A.V. Arzhannikova:** Writing – review & editing, Validation. **R.N. Kurbanov:** Resources.

#### Declaration of Competing Interest

The authors declare that they have no known competing financial interests or personal relationships that could have appeared to influence the work reported in this paper.

#### Data availability

No data was used for the research described in the article.

#### Acknowledgements

Special thanks to Dr. Daria Semikolenykh for the description of the OSL dating procedure. The reported study was mostly funded by the Russian Foundation for Basic Research grant № 20-55-15002. Remote sensing analysis of the relief features was possible thanks to the TanDEM-X project DEM\_GEOL1188. The study of terrace sections and analysis of terrace levels in the Tunka Depression to assess tectonic or climatic incision factors was supported by the Russian Science Foundation (grant no. 22-17-00049). The work was conducted using equipment and infrastructure of the Centre for Geodynamics and Geochronology at the Institute of the Earth's Crust, Siberian Branch of the Russian academy of Sciences (grant no 075-15-2021-682).

#### References

Adamenko, O.M., Adamenko, R.S., Belov, V.A., et al., 1984. About the age of molasse strata of the Baikal rift zone from mammal fauna determinations. In: *Environment*

- and Life at the Turn of Epochs in the Cenozoic in Siberia and the Far East. Nauka, Novosibirsk, pp. 189–193. In Russ.
- Adamenko, O.M., Belova, V.A., Popova, S.M., et al., 1975. Biostratigraphy of Late Pleistocene deposits of the Tunka Depression. *Geology and geophysics*. № 6. P. 78–85. (In Russ.).
- Alexeev, S., Alexeeva, L., Kononov, A., 2014. Cryogenic deformation structures in Late Cenozoic unconsolidated sediments of the Tunka depression in the Baikal Rift Zone. *Permafrost. Periglacial Process.* 25, 117–126.
- Anderson, B.G., Droser, M.L., 1998. Ichnofabric sand geometric configurations of Ophiomorpha within a sequence stratigraphic framework: an example from the Upper Cretaceous US western interior. *Sedimentology* 45, 379–396.
- Arzhannikova, A., Larroque, C., Ritz, J.-F., De' verchere, J., Ste'phan, J.-F., Arzhannikov, S., San'kov, V., 2004. Geometry and kinematics of recent deformation in the Mondy-Tunka area (south-westernmost Baikal rift zone, Mongolia-Siberia). *Terra Nova*, v. 16, № 5, p. 265.272.
- Arzhannikov, S., Braucher, R., Jolivet, M., Arzhannikova, A., Vassallo, R., Chauvet, A., et al., 2012. History of late Pleistocene glaciations in the central Sayan-Tuva Upland (southern Siberia). *Quat. Sci. Rev.* 49, 16–32.
- Arzhannikov, S., Arzhannikova, A., Ivanov, A., Demonterova, E., Yakhnenko, A., Gorovoy, V., Jansen, J., 2021a. (1). Lake Baikal highstand during MIS 3 recorded by palaeo-shorelines on Bolshoi Ushkaniy Island. *Boreas* 50, 101–113. <https://doi.org/10.1111/bor.12464>. ISSN 0300-9483.
- Arzhannikov, S.G., Braucher, R., Jolivet, M., Arzhannikova, A.V., 2015. Late Pleistocene glaciations in southern East Sayan and detection of MIS 2 end moraines based on beryllium ( $^{10}\text{Be}$ ) dating of glacier complexes. *Russ. Geol. Geophys.* 56, 1509–1521.
- Arzhannikov, S. G., Brochet, R., Arzhannikova, A.V., Ivanov, A.V., Demonterova, E. I., Burle, D., Yanson, D., 2021 (2). New data on the age of the terraces of Bolshoy Ushkaniy Island (Lake Baikal) /Faulting in the lithosphere and related processes: Tectonophysics analysis: abstracts of reports of the All-Russian meeting dedicated to the memory of Professor S. I. Sherman. Irkutsk / FGBUN IZK SB RAS; FGBOU VO "IGU"; ed. by K. Zh. Seminsky. Irkutsk, Russia: IGU Publishing House. Pp. 59–60. (In Russ.).
- Arzhannikov, S.G., Ivanov, A.V., Arzhannikova, A.V., Demonterova, E.I., Jolivet, M., Buyantuev, V.A., Oskolkov, V.A., Voronin, V.I., 2016. The most recent (682–792 CE) volcanic eruption in the Jombolok lava field, East Sayan, Central Asia triggered exodus of Mongolian pre-Chinggis Khaan tribes (778–786 CE). *J. Asian Earth Sci.* 125, 87–99. <https://doi.org/10.1016/j.jseas.2016.05.017>.
- Arzhannikov, S.G., Ivanov, A.V., Arzhannikova, A.V., Demonterova, E.I., Jansen, J.D., Preusser, F., Kamenetsky, V.S., Kamenetsky, M.B., 2018. Catastrophic events in the Quaternary out flow history of Lake Baikal. *Earth Sci. Rev.* 177, 76–113.
- Arzhannikova, A., Arzhannikov, S., Braucher, R., Jolivet, M., Aumaître, G., Bourlès, D., Keddadouche, K., 2018. Morphotectonic analysis and  $^{10}\text{Be}$  dating of the Kyngarga river terraces (southwestern flank of the Baikal rift system, South Siberia). *Geomorphology* 303, 94–105. <https://doi.org/10.1016/j.geomorph.2017.11.019>.
- Arzhannikova, A., Arzhannikov, S., Jolivet, M., Vassallo, R., Chauvet, A., 2011. Pliocene to Quaternary deformation in South East Sayan (Siberia): Initiation of the Tertiary compressive phase in the southern termination of the Baikal Rift System. *Journal of Asian Earth Sciences* 40, 581–594. <https://doi.org/10.1016/j.jseas.2010.10.111>.
- Arzhannikova, A.V., Arzhannikov, S.G., Ritz, J.-F., Chebotarev, A.A., Yakhnenko, A.S., 2023. Earthquake geology of the Mondy Fault (SW Baikal Rift, Siberia). *J. Asian Earth Sci.* 248, 105614 <https://doi.org/10.1016/j.jseas.2023.105614>.
- Arzhannikova A., Ritz J.-F., Larroque C., Antoine P., Arzhannikov S., Chebotarev A., Stephan J.-F., M. Massault, Michelot J.-L., 2020. Cryoturbation versus tectonic deformation along the southern edge of the Tunka Basin (Baikal Rift System), Siberia: New insights from an integrated morphotectonic and stratigraphic study. *J. Asian Earth Sci.* 204 [doi.org/10.1016/j.jseas.2020.104569](https://doi.org/10.1016/j.jseas.2020.104569).
- Berdnikov, I.M., Rogovskoi, E.O., Lohkov, D.N., Kuznetsov, A.M., Kogai, S.A., Lipnina, E. A., Berdnikova, N.E., Saveliev, N.A., Sokolova, N.B., Ulanov, I.V., 2017. New Radiocarbon Data for the Neolithic Complexes of Multilayered Sites in Tunka Valley and Angara Region. Eurasia in the Cenozoic. *Stratigraphy, Paleocology, Cultures* 6. Pp. 220–230. (In Russ.).
- Buatois, L. A. and Mangano, M. G., 2011. *Ichnology: Organism-substrate Interactions in Space and Time*. Cambridge University Press, Cambridge. P. 358.
- Bulmasov, A.P., 1963. Structures and gravity anomalies of cryogenic origin in Pribaikalie. *Geol. Geophys.* 2, 75–85. In Russian.
- Bulmasov, A.P., 1967. Some results of geophysical study of the Baikal region. *Geological results of geophysical research in Siberia and the Far East*. N.: Nauka. Pp.360-372.
- Buylaert, J.P., Jain, M., Murray, A.S., Thomsen, K.J., Thiel, C., Sobhati, R., 2012. A robust feldspar luminescence dating method for Middle and Late Pleistocene sediments // *Boreas* 41, 435–451.
- Chebotarev, A., Arzhannikova, A., Arzhannikov, S., 2021. Long-term throw rates and landscape response to tectonic activity of the Tunka Fault (Baikal Rift) based on morphometry. *Tectonophysics* 810, 228864. <https://doi.org/10.1016/j.tecto.2021.228864>.
- Chipizubov, A.V., Smekalin, O.P., 1999. Fault scarps and the causative prehistoric earthquakes in the main Sayan fault zone. *Russ. Geol. Geophys.* 40 (6), 921–931.
- Chipizubov, A.V., Smekalin, O.P., Semenov, R.M., 2003. Fault scarps and prehistoric earthquakes in the Tunka fault (southwestern Baikal region). *Russ. Geol. Geophys.* 44 (6), 587–602.
- Enikeyev, F., 2019. Sandy massifs of the Chara depression (northern transbaikalia). Notes of the Transbaikalian Branch of the Russian Geographical society. Chita, October 23, (In Russ.).
- Gilbert, G. K., 1890. Lake Bonneville, Monogr. U.S. Geological Survey, vol. 1, U.S. Geological Survey, Washington, D. C., <https://doi.org/10.3133/m1>.
- Guérin, G., Mercier, N., Adamic, G., 2011. Dose-rate conversion factors: update. *Ancient TL* 29, 5–8.

- Hassan, A., Rasskazov, S.V., Chuvashova, I.S., Yasnygina, T.A., Titova, L.A., Kulagina, N. V., Usoltseva, M.V., 2020. Identifying upper miocene – lower pliocene lacustrine sediments in dry Tunka basin of the Baikal rift zone. *Geodynam. Tectonophys.* 11 (2), 262–284. <https://doi.org/10.5800/GT-2020-11-2-0473>. In Russ.
- Hassan, A., Rasskazov, S.V., Chuvashova, I.S., Al-Hamdu, A., 2021. Structural development of the central Baikal Rift System: similarities and differences of the Barguzin and Tunka Valleys. *Geol. Environ.* 1 (1).
- Highlands of the Baikal region and Transbaikalia, 1974. N.A. Florensov (Eds.). M.: Nauka. P. 359.
- Howard, J.D., Frey, R.W., 1984. Characteristic trace fossils in nearshore to offshore sequences. Upper Cretaceous of east central Utah. *Can. J. Earth Sci.* 21, 200–219.
- Huntley, D.J., Baril, M.R., 1997. The K content of the K-feldspars being measured in optical dating or in thermoluminescence dating // *Ancient TL* 15 (1), 11–13.
- Isaev V.P., 2007. 'Mud' volcanoes in the basins of the Baikal rift system. *Geology and minerals of East Siberia*. ISU Publishing House, Irkutsk. Pp. 133–137. (In Russ.).
- Isaev V.P., 2016. Petroleum Prospects of Intermountain Depressions in Buryatia. GEO, Novosibirsk. P. 165. (In Russ.).
- Firsov, L.V., Panychev, V.A., Orlova, L.A., 1985. The catalogue of radiocarbon dates. IGG SB AS USSR, Novosibirsk (in Russ).
- Jolivet M., De Boissgrillier T., Petit C., Fournier M., San'kov V.A., Ringenbach J.-C., Byzov L.M., Miroshnichenko A.I., Kovalenko S.N., Anisimova S.V., 2009. How old is the Baikal rift zone? Insight from apatite fission track thermochronology. *Tectonics*. V. 28. doi:10.1029/2008 TC002404.
- Jolivet M., Arzhannikov S., Arzhannikova A., Chauvet A., Vassallo R., Braucher R., 2013. Geomorphic Mesozoic and Cenozoic evolution in the Oka-Jombolok region (East Sayan ranges, Siberia). *Journal of Asian Earth Sciences*. V. 62. Special Issue SI. Pp. 117–133. Doi:10.1016/j.jseas.2011.09.017.
- Kolomiets, V.L., 1994. Reconstruction of sedimentation conditions for the sand series in the Lower Turka Basin. In: *Baikal and Mountains Around It (Cenozoic geology, geomorphology, neotectonics and geological natural relics)*. Abstract of the Irkutsk geomorphological seminar, Irkutsk, pp. 95–96.
- Kolomiets, V. L., 1998. Reconstructions of parameters of paleo-streams based on fossil sediments. *Bulletin of the Buryat University. Series 3: Geography, geology*. V.2. Ulan-Ude: Publishing House of BSU. Pp. 92–100. (In Russ.).
- Kolomiets V.L., 2010. Sedimentogenesis of the Pleistocene aquatic complex and conditions for the formation of non-metallic raw materials of the dry depressions of the Baikal rift zone. Summary of the PhD Thesis, Irkutsk. 18 pp. (In Russ.).
- Kolomiets V.L., 2019. Sedimentogenesis of sedimentary strata of the Badar massif in the Tunka rift valley. Rifting, orogenesis, and accompanied processes. *Proceedings of the IV All-Russian symposium with participation of foreign scientists, dedicated to the 90th anniversary of Academician Nikolay Logatchev Irkutsk*, October 14–15. Irkutsk: Institute of the Earth's Crust SB RAS, 2019. Pp. 78–79.
- Kolomiets V. L., 2021. Pleistocene lithogenesis of the dry-land depressions of Baikal Siberia. Problems of regional geology of the West of the East European Platform and adjacent territories: materials of the II International Scientific Conference, Rep. Belarus, Minsk, February 16. Belarusian State University. Minsk. BSU. Pp. 71–76. (In Russ.).
- Kozyrev, A., Shchetnikov, A., Klemenev, A., Filinov, I.A., Fedorenko, A., White, D., 2014. The early upper palaeolithic of the Tunka rift valley, lake Baikal region, Siberia. *Quat. Int.* 348, 4–13.
- Krивonogov, S.K., Safonova, I.Y., 2017. Basin structures and sediment accumulation in the Baikal Rift Zone: Implications for Cenozoic intracontinental processes in the Central Asian Orogenic Belt. *Gondw. Res.* 47, 267–290.
- Krивonogov S.K., 2010. Late Pleistocene to Holocene Sedimentation in the basins of the Baikal Rift Zone. Summary of the Thesis for the Degree of Doctor of Geology and Mineralogy, Irkutsk. 32 pp. (In Russ.).
- Kul'chitsky A.A., Osadchy S.S., Misharina V.A., Popova S.M., Chernyaeva G.P., Fileva T. S., Orlova L.A., Krивonogov S.K., 1994. Results of study of Tunka Basin of sandy sites (Bely Yar I and Bely Yar-II) on Baikal and its mountain surround. *Irkutsk Geomorphology Seminar IGU*. Pp. 100–103. (In Russ.).
- Kurbanov, R.N., Ulyanov, V.A., Anoykin, A.A., Pavlenok, G.D., Semikolennykh, D.V., Kharevich, V.M., Taymagambetov, Z.K., Murray, A.S., 2019. The first luminescence chronology of the Initial Upper Paleolithic of Eastern Kazakhstan (case study of the Ushbulak archaeological site) // *Vestnik Moskovskogo universiteta. Seriya 5. Geografiya*. 6, 29–39 in Russian.
- Larroque, C., Ritz, J.F., Stéphan, J.F., Sankov, V., Arzhannikova, A., Calais, E., Deverchere, J., Loncke, L., 2001. A compression–extension interaction on the Siberian-Mongolian border. Preliminary analysis of recent and actual deformations in the Tunka basin. *Earth Planet. Sci.* 332, 177–184.
- Logachev, N.A., 1958. Cenozoic continental deposits in the depression of the Baikal type. *Izvestia AN SSSR. Geological series* 4, 18–29. In Russian.
- Logachev, N.A., 1968. Sedimentary and volcanogenic formations of the Baikal rift zone. In: Florensov, N.A. (Ed.), *Baikal rift*. Nauka, Moscow, pp. 72–101. In Russ.
- Logachev, N.A., 2003. History and geodynamics of the Baikal rift. *Geol. Geophys.* 44 (5), 391–406. In Russ.
- Logatchev, N.A., Zorin, Y.A., 1987. Evidence and causes for the two-stage development of the Baikal rift. *Tectonophys.* 143, 225–234.
- MacEachern, J.A., Pemberton, S.G., Gingras, M.K., Bann, K.L., 2007. The ichnofacies concept: a fifty-year retrospective. In: Miller III, W. (Ed.), *Trace Fossils. Concepts, Problems, Prospects*. Elsevier, Amsterdam, pp. 50–75.
- Makarov, S.A., Ryzhov, Y.V., Kobylkin, D.V., Ryashchenko, T.G., 2016. Formation of river terraces in conditions of high seismicity. *Geogr. Nat. Resour.* 37 (1), 64–70.
- Maksimov F.E., Savelyeva L.A., Laukhin S.A., Larin S.I., Arslanov H.A., Kuznetsov V.Yu., Grigoriev V.A., Starikova A.A., 2015. Geochronometric characteristics and conditions of formation of lake-alluvial strata in the section Bely Yar-II (Tunka Basin). *Fundamental problems of the quarter, the results of the study and the main directions for further research*. Irkutsk: Publishing House of the Institute of Geography SB RAS. Pp. 297–299.
- Maksimov, F.E., Savelyeva, L.A., Laukhin, S.A., Petrov, A.Y., Popova, S.S., Larin, S.I., Kobylkin, D.V., Kuznetsova, V.Y., Grigoryev, V.A., Levchenko, S.B., Yakimova, K.S., 2020. New Evidence on the Age and Formation Conditions of Pleistocene Deposits in the Eastern Part of the Tunka Depression. *Geogr. Nat. Resour.* 41 (3), 266–277. <https://doi.org/10.1134/S1875372841030087>.
- Margold, M., Jansen, J.D., Codilean, A.T., Preusser, F., Gurinov, A., Fujioka, T., Fink, D., 2018. Repeated megafloods from glacial Lake Vitim, Siberia, to the Arctic Ocean over the past 60,000 years. *Quart. Sci. Rev.* 187, 41–61.
- Martinson, G.G., 1948. Fossil sponges from the Tunka basin in Pribaikalie. *Doklady AN SSSR, New Series XI* 5, 56–60. In Russ.
- Mats, V.D., 1993. The structure and development of the Baikal rift depression. *Earth – Sci. Rev.* 34, 81–118.
- Matz, V.D., Fujii, S.h., Mashiko, K., et al., 2002. To the paleohydrology of Baikal in relation to neotectonics. *Geol. Geophys.* 43 (2), 142–154.
- Mazilov, V.N., Lomonosova, T.K., Klimanova, V.M., 1972. *Lithology of Tertiary Sediments in the Southwestern Baikal Rift Zone*. Nauka, Moscow. In Russ.
- Mikuláš R., Dronov A., 2006. *Palaeoichnology. Introduction to the study of trace fossils*. Institute of geology, Academy of Sciences of Czech Republic, p. 122, Prague.
- Molnar, P., Tapponnier, P., 1975. Cenozoic Tectonics of Asia: Effects of a Continental Collision. *Science* 189, 419–426. <https://doi.org/10.1126/science.189.4201.419>.
- Murray, A.S., 1996. Developments in optically transferred luminescence and photo-transferred thermoluminescence dating: application to a 2000-year sequence of flood deposits. *Geochim. Cosmochim. Acta* 60, 565–576.
- Murray, A.S., Marten, R., Johnston, A., Martin, P., 1987. Analysis for naturally occurring radionuclides at environmental concentrations by gamma spectrometry // *Journal of Radioanalytical and Nuclear Chemistry. Articles*. 115 (2), 263–288.
- Murray, A.S., Helsted, L.M., Autzen, M., Jain, M., Buylaert, J.P., 2018. Measurement of natural radioactivity: Calibration and performance of a high-resolution gamma spectrometry facility. *Radiat. Meas.* 15, 215–220.
- Murray, A.S., Lee, J., Arnold, J.-P., Guérin, G., Qin, J., Singhvi, A.K., Smedley, R., Thomsen, K.J., 2021. Optically stimulated luminescence dating using quartz // *Article number: 71 Nat. Rev. Methods Primers* 1.
- Opekunova M.Y., Kobylkin D.V., 2009. Morphology of river terraces of the Irkut River basin. *Geography and Natural Resources*, No. 4.
- Osadchy S.S., 1995. Traces of the maximum transgression of Baikal. *Geography and natural resources*. V.1. Novosibirsk. Nauka Publishing House. Pp.179–189. (In Russ.).
- Parfeevets, A.V. and San'kov, V.A., 2006. Geodynamic conditions of evolution of the Tunka branch in the Baikal Rift system. *Geotectonics* 5, 377–398.
- Popova, S.M., Mats, V.D., Chernyaeva, G.P., et al., 1989. *Paleolimnological Reconstructions (Baikal Rift Zone)*. Siberian Branch, Nauka, Novosibirsk, p. 110. In Russ.
- Prescott, J.R., Hutton, J.T., 1994. Cosmic ray contributions to dose rates for luminescence and ESR dating: large depths and long-term time variations. *Radiat. Meas.* 23, 497–500.
- Rasskazov S.V., Sankov V.A., Ruzhich V.V., Smekalin O.P., 2010. *Cenozoic Continental Rifting: Guide of Geological Excursions in Tunka rift basin*. Institute of the Earth's Crust SB RAS, Irkutsk, 40 p. (In Russ.).
- Ravsky, E.I., Alexandrova, L.P., Vangengeim, E.A., Gerbova, V.G., Golubeva, L.V., 1964. *Anthropogene Deposits of Southern East Siberia*. Nauka Press, Moscow, p. 105. In Russ.
- Ravsky, E.I., 1972. *Sedimentation and climates of Inner Asia in Anthropogenic*. Moscow. P. 336.
- Reineck, H.-E., Singh, I.B., 1980. *Depositional Sedimentary Environments*. Springer-Verlag, Berlin/New York, p. 549.
- Ritz, J.-F., Arzhannikova, A., Vassallo, R., Arzhannikov, S., Larroque, C., Michelot, J.-L., Massault, M., 2018. Characterizing the present-day activity of the Tunka and Sayan faults within their relay zone (western Baikal Rift system, Russia). *Tectonics* 37 (5), 1376–1392.
- Scruton, P.C., 1955. Sediments of the eastern Mississippi delta. In *Finding ancient shorelines*. SEPM Spec. Publ. 3, 21–51.
- Seismotectonics and seismicity of the rift system of the Baikal region, 1968. Solonenko V. P. (Eds). USSR Academy of Sciences, Siberian Branch, Institute of the Earth's Crust. Moscow : Nauka, 220 p.
- Semeney, E.Y., Shchetnikov, A.A., Filinov, I.A., Vesheva, S.V., 2014. Formation conditions and correlation of upper Neo-Pleistocene reference section deposits in the south of eastern Siberia by lithochemical data. *Bulletin of IrStU* 9, 56–62.
- Semeney E.Yu., 2015. Stratigraphy and correlation of sediments Upper Pleistocene of the Southern Siberian platform and Tunka Rift. Summary of the PhD Thesis, Irkutsk. 23 pp. (In Russ.).
- Shchetnikov, A.A., 2017. Inversion morphotectonics in the depressions of the Tunka rift (South-Western Baikal region). *Geol. Geophys.* 58 (7), 972–985.
- Shchetnikov A.A., Ufimtsev G.F., 2004. Relief structure and recent tectonics of the Tunka rift (southwestern Baikal region). *Nauchnyi Mir*, Moscow. 160 p. (In Russ.).
- Shchetnikov, A.A., White, D., Filinov, I.A., Rutter, N., 2012. Late Quaternary geology of the Tunka rift basin (Lake Baikal region), Russia. *J. Asian Earth Sci.* 46, 195–208.
- Shchetnikov, A.A., Semenei, E.Y., Filinov, I.A., Khenzykhenova, F.I., 2015. New data on the Late Pleistocene stratigraphy and paleoenvironment of the southwestern Baikal area (Siberia). *Quat. Int.* 355, 65–79.
- Shchetnikov, A.A., Bezrukova, E.V., Kazansky, A.Y., Matasova, G.G., Ivanova, V.V., Danukalova, G.A., Filinov, I.A., Khenzykhenova, F.I., Osipova, E.M., Berdnikova, N. E., Berdnikov, I.M., Rogovskoy, E.O., Lipnina, E.A., Vorobyeva, G.A., 2019. Upper Paleolithic site Tuyana - a multi-proxy record of sedimentation and environmental history during the Late Pleistocene and Holocene in the Tunka rift valley, Baikal region. *Quat. Int.* 534, 138–157. <https://doi.org/10.1016/j.quaint.2019.02.043>.

- Sherman S.I., Medvedev M.E., Ruzgich V.V. et al., 1973. Tectonics and volcanism in the south-western part of the Baikal rift zone. Publishing House Nauka, Novosibirsk, 1973. 136 p. (In Russ.).
- Smekalin, O.P., 2008. The study of the paleoseismic deformations of the Southern Pribaikalie. IPE RAS, Moscow, p. 101.
- Strom A.L., 2022. Stone avalanches of Central Asia: structural features, patterns of formation and catastrophic consequences. Summary of the Thesis for the Degree of Doctor of Geology and Mineralogy, Moscow. 44 pp. (In Russ.).
- Tectonics and Volcanism of the Southwestern Part of the Baikal Rift Zone, 1973. Florensov N.A. (Eds.), Nauka, Novosibirsk, 136 p. (In Russ.).
- Thiel, C., Buylaert, J.P., Murray, A., Terhorst, B., Hofer, I., Tsukamoto, S., Frechen, M., 2011. Luminescence dating of the Stratzing loess profile (Austria) – testing the potential elevated temperature post-IR IRSL protocol. *Quat. Int.* 234, 23–31.
- Ufimtsev, G.F., Janotta, A., Perevalov, A.V., Radke, U., Rezanova, V.P., Vogt, T., Shchetnikov, A.A., 1999. Aeolian landscapes of the Tunka basin. *Geogr. Nat. Resour.* 1, 65–70.
- Ufimtsev, G.F., Shibanova, I.V., Kulagina, N.V., Mashchuk, I.M., Perevalov, A.V., Rezanova, V.P., Vogt, T., Ignatova, N.V., Misharina, V.A., 2002. Upper Pleistocene and Holocene deposits of the Tunka rift. *Stratigr. Geol. Correl.* 10 (3), 90–99.
- Ufimtsev, G.F., Perevalov, A.V., Rezanova, V.P., Kulagina, N.V., Mashchuk, I.M., Shchetnikov, A.A., Rezanov, I.N., Shibanova, I.V., 2003. Radiothermoluminescence dating of Quaternary sediments of the Tunka rift. *Geol. Geophys.* 44 (3), 226–232.
- Ufimtsev, G.F., Shchetnikov, A.A., Filinov, I.A., 2009. Inversions in the contemporary geodynamics of the Baikal rift zone. *Geol. Geophys.* 50 (7), 798–810.
- Vasilyev, S.V., Borutskaya, S.B., Rogovskoi, E.O., Berdnikova, N.E., Lipnina, E.A., Berdnikov, I.M., 2017. Otchet Ob Antropologicheskikh Nakhodkakh Na Territorii Paleoliticheskoy Stoyanki Tuyana V Tunkinskoy Riftovoy Doline (Yugo-Zapadnyy Pribaikal'ye) (Report on Anthropological Finds on the Paleolithic Site Tuyana in the Tunka Rift Valley (Southwestern Cis-Baikal)). *Bulletin of the Irkutsk State University. Geoarchaeology, Ethnology, and Anthropology Series* 22, 150–165 (in Russ.).
- Vogt, T., Janotta, A., Radtke, U., 1998. Morphologische Studien in Sedimenten des Spätpleistozän. Frühholozän im Gebiet des Baikalriffs (Südostsibirien). *Kölner Geographische Arbeiten* 70, 95–102.
- Vogt, H., Vogt, T., 2007. Morphotectonic evolution of two depressions at the southern border of the Baikal rift system. *Geomorphology* 86 (3), 480–495.
- VSEGEI, 1965. Geological map 1:200,000 East Sayan series, sheet M-47-VI. Leningrad.
- VSEGEI, 1966. Geological map 1:200,000 East Sayan series, sheet M-48-II. Leningrad.
- VSEGEI, 1969. Geological map 1:200,000 East Sayan series, sheet M-48-I. Leningrad.
- Vyrkin, V.B., Opekunova, M.Y., 2001. Morphology and structure of the Irkut river basin. Ecological and geographical studies in river basins. Voronezh. 25–28. In Russ.
- Zamaraev, S.M., 1975. Gravitational tectogenesis in the sedimentary thickness of the Lake Baikal depression. Circulation of matter and energy in lake reservoirs. Nauka, Novosibirsk, pp. 418–423.
- Zonenshain, L.P., Savostin, L.A., 1981. Geodynamics of the Baikal rift zone and plate tectonics of Asia. *Tectonophysics* 76 (1–2), 1–45.

### Further reading

- Bezrukova E.V., Kulagina N.V., Reshetova S.A., Shchetnikov A.A., Krainov M.A., Filinov I.A., 2022. Environment of the Oka Plateau (East Sayan Mountains) in the Late glacial and Holocene: a case study of a complex record from the Lake Khikushka sediments. *Geomorfologiya* 53 (3) Pp. 61-73. (In Russ.).